POLITECNICO DI TORINO
Repository ISTITUZIONALE

Ranking critical bridges in wide-area road networks through iterative macroscopic traffic simulation

Original
Ranking critical bridges in wide-area road networks through iterative macroscopic traffic simulation / Charlang Bakhtyari, A., Deflorio, F.. - In: TRANSPORTATION RESEARCH. PART A, POLICY AND PRACTICE. - ISSN 0965-8564. - 214:(2026). [10.1016/j.tra.2026.105266]

Availability:
This version is available at: 11583/3015768 since: 2026-09-21T13:29:26Z

Publisher:
Elsevier

Published
DOI:10.1016/j.tra.2026.105266

Terms of use:

This article is made available under terms and conditions as specified in the corresponding bibliographic description in the repository

Publisher copyright

(Article begins on next page)

25 October 2026

Transportation Research Part A 214 (2026) 105266

Contents lists available at ScienceDirect

Transportation Research Part A

journal homepage: www.elsevier.com/locate/tra

Ranking critical bridges in wide-area road networks through iterative macroscopic traffic simulation☆

Amirehsan Charlang Bakhtyari *, Francesco Deflorio

DIATI, CARS@POLITO, Politecnico di Torino, Duca degli Abruzzi 24, 10129 Torino, Italy

ARTICLE INFO

Keywords:
Vulnerability
Transportation resilience
Road network
Traffic simulation
Mobility disruptions
Disaster mobility preparedness

ABSTRACT

Bridge failures in case of disruptive events can lead to severe mobility interruptions and losses in regional connectivity. This study proposes a scalable and computationally efficient network modeling methodology to support the prioritization of bridge monitoring and retrofitting under resource constraints by integrating publicly available datasets, hazard information, and simplified incremental macroscopic traffic simulation. Using Alessandria, Italy, as a case study, baseline and disrupted road network scenarios were generated, where flood-exposed bridge edges were iteratively closed one at a time to represent flood-induced disruptions. An origin–destination matrix was estimated to assess traffic redistribution under each disruption scenario. Traffic performance indicators were then used to quantify the impacts of bridge-edge closures on regional mobility, and the analysis was extended to complete physical-bridge closures. The findings reveal that while local bridges may produce high relative increases in travel time, motorway bridges generate disproportionately large absolute impacts due to their high traffic volumes, underscoring their crucial role in maintaining regional connectivity. The principal criticality patterns were preserved when complete physical bridges were closed, while comparison with a topological assessment highlighted the importance of considering traffic demand and route redistribution. A traffic-demand sensitivity analysis further confirmed the robustness of the identified critical bridges under variations in motorway crossing demand.

1. Introduction

Road networks are fundamental to the functioning of societies in both developed and developing countries. They play a critical role in facilitating daily mobility, enabling the transportation of goods, and acting as essential lifeline systems during emergencies by maintaining connectivity. Beyond their contribution to normal urban operations, road networks are indispensable for emergency response, the protection of economic assets, and the restoration of other critical infrastructure systems. As the backbone of transportation infrastructure, they are central to ensuring societal resilience and continuity, thereby underscoring their vital role in sustaining modern life (Mattsson and Jenelius, 2015; Pregnolato et al., 2017; Zhao et al., 2022; Li et al., 2024).

However, road networks increasingly face challenges due to natural hazards such as floods, earthquakes, tsunamis, hurricanes, and volcanic eruptions, as well as rapid urbanization and the growing interdependence of infrastructure systems (Pregnolato et al., 2017; Aghababaei et al., 2021; Boeing and Ha, 2024). Within this context, bridges, being critical components of road networks, are

☆ This article is part of a special issue entitled: 'Resilience & Regional Econ Dev' published in Transportation Research Part A.

* Corresponding author.
E-mail address: amirehsan.charlang@polito.it (A. Charlang Bakhtyari).

https://doi.org/10.1016/j.tra.2026.105266

Available online 15 September 2026
0965-8564/© 2026 The Author(s). Published by Elsevier Ltd. This is an open access article under the CC BY-NC-ND license (http://creativecommons.org/licenses/by-nc-nd/4.0/).

particularly vulnerable to natural disasters, such as flooding events and seismic actions, as well as technological and manmade disasters. Failures or damage to these structures can significantly disrupt connectivity, impede rescue efforts, and delay post-disaster recovery, thereby affecting overall societal resilience and mobility. A notable example is the collapse of the Morandi Bridge in Genoa in 2018, where a section of approximately 240 m of the deck failed near a critical pier, causing severe disruption to regional connectivity and traffic flows between northern Italy and southern France, along with significant human and economic losses. The event highlighted how localized structural deficiencies, exacerbated by long-term degradation, can trigger sudden network-wide impacts, demonstrating the critical role of bridges as bottlenecks in road systems (Lanari et al., 2020).

Berdica (2002) introduced the concept of road network vulnerability, defining it as the susceptibility of road networks to incidents that substantially reduce their serviceability. More broadly, vulnerability refers to the propensity of a system to experience disruptions or failures that compromise its functionality. Resilience refers to a system's capacity to adapt to adverse events and minimize potential losses. In transportation systems, resilience is typically described as the ability to restore acceptable levels of service within a reasonable timeframe following a disruption (Westrum, 2006; Ganin et al., 2017). The most vulnerable elements of a network often require focused attention and timely interventions to reduce the scale of disruptions and expedite recovery. In the context of civil infrastructure, resilience is characterized by four key attributes: robustness, rapidity, redundancy, and resourcefulness. Robustness is the system's ability to maintain a minimum level of function following a disruptive event. Rapidity measures the speed of recovery. Redundancy refers to the extent to which substitute components or pathways are available within the system. Resourcefulness denotes the system's capability to identify challenges, prioritize actions, and allocate resources effectively in response to a crisis (Bruneau et al., 2003).

Flooding, in particular, has a pronounced impact on road infrastructure, leading to widespread mobility disruptions, structural damage, and delays in recovery efforts. These disruptions not only pose direct threats, such as vehicle-related fatalities and road closures, but also result in indirect consequences including prolonged emergency response times, increased congestion, and diminished network efficiency and resilience (Pyatkova et al., 2019; Evans et al., 2020).

Historical events highlight the vulnerability of road infrastructure, particularly bridges, to extreme flooding. For instance, the 1994 Piedmont flood in Italy resulted in 70 fatalities, displaced over 2,200 people, and severely impacted the provinces of Cuneo, Asti, and Alessandria. The disaster caused widespread damage estimated at over 12 billion USD, with nearly one-third affecting public infrastructure and agriculture. Approximately 150 bridges either collapsed or sustained severe damage, intensifying the disruption to road networks (Buzzi et al., 1998; Mandarino et al., 2021). More recently, in October 2024, the Valencia region in Spain experienced one of its most catastrophic meteorological events of the century, a DANA (Depresión Aislada en Niveles Altos), marked by torrential rainfall and flash flooding. The resulting infrastructural damage was extensive, with repair costs estimated at €2.6 billion. Infrastructures including roads and bridges sustained severe damage. The event disrupted high-speed rail services, derailed a train near Málaga, damaged over 100,000 vehicles, and cut critical transportation corridors such as the motorway A-3/E-901 and motorway A-7/E-15. The response highlighted the community's resilience through volunteer mobilization but also revealed significant deficiencies in pre-disaster planning and infrastructure resilience (Galvez-Hernandez et al., 2025; Wikipedia, 2024).

The increasing frequency and intensity of extreme climate events underscore the need for practical disaster preparedness, particularly through the implementation of bridge monitoring and retrofitting strategies aimed at enhancing the resilience of road networks to natural disasters. These measures are vital for reducing structural damage, preventing scour-induced failures, and maintaining service continuity both during and after disruption events. However, monitoring and retrofitting all vulnerable bridges often requires high economic resources. Consequently, it can be efficient for transportation authorities and decision-makers to identify and prioritize the most critical bridges, those whose failure would lead to the greatest network disruption in terms of accessibility for the area. This calls for the development of methodologies to support informed decision-making and the efficient allocation of limited resources for resilience enhancement.

Several methodologies have been proposed to assess the criticality of road network links and bridges. Early approaches predominantly relied on spatial and topological analyses, emphasizing the structure and connectivity of road networks. These methods are relatively straightforward to implement and effective for rapid scenario evaluations, as they do not require detailed link attributes or traffic flow data. A common preliminary method involves identifying bridge edges, defined as links whose removal would disconnect the network (Gao et al., 2019; Ouyang et al., 2019; Deflorio et al., 2024). However, such topological methods are limited in their ability to capture traffic dynamics, demand distribution, and congestion effects, which play a fundamental role in determining the actual impact of disruptions on network performance (Taylor, 2017). Recent studies have highlighted the importance of incorporating traffic demand into vulnerability analysis. For instance, Charlang Bakhtyari et al. (2025) demonstrated that accounting for traffic demand influences the assessment of network vulnerability to disruptions, confirming that purely topological approaches are more suitable for preliminary screening than for comprehensive impact assessments.

Beyond spatial and topological analyses, a wide range of optimization-based techniques and decision-support frameworks have been developed to incorporate additional dimensions such as functionality, economic cost, and social impact. For instance, Akbari and Sayarshad (2022) proposed a mathematical model for the coordinated, simultaneous restoration of road infrastructure and distribution of relief supplies, aiming to minimize the time required for a relief team to reach the final critical demand node following a sudden-onset disaster. Their model integrates the actions of two teams, one focused on delivering essential supplies and the other on clearing blocked road links, while accounting for stochastic blockage durations to improve post-disaster logistics planning. Similarly, Peng et al. (2024) addressed the sequencing of concurrent restoration activities in disrupted infrastructure networks through a bilevel network flow model. They introduced a discrete dynamic system to capture time-dependent traffic and developed a restoration network (R-Net), where restoration sequences are represented as paths from source to sink. The optimal sequence is obtained by selecting the minimum-cost path, with edge costs reflecting both system disutility and restoration time. This model facilitates concurrent repair

activities by allowing work crews to begin new tasks immediately upon completing previous ones. Zamanifar and Hartmann (2021) proposed a multi-stage decision-making framework for transportation network recovery planning, emphasizing the identification and evaluation of relevant decision attributes through both compensatory and non-compensatory decision rules. Drawing from literature and expert input, they identified 57 candidate attributes and applied a three-stage evaluation process using multi-attribute decision-making techniques. The study resulted in a ranked list and a recommended set of six key attributes for disaster recovery planning in road network of Tehran: access level to service-providing nodes, integration of link travel delay and traffic flow, travel time improvement per unit of recovery duration, travel time improvement per unit of resources, centrality measures, and link capacity. Notably, these attributes are intended to function as an interdependent set. The findings offer valuable insights into the priorities and trade-offs involved in post-disaster reconstruction and recovery of transportation networks.

Other studies have employed multi-criteria and utility-based approaches to address the complexity of post-disaster infrastructure decision-making. Mashrur and Kameshwar (2025) applied a non-dominated sorting algorithm to rank links and paths based on multiple indicators, aiming to ensure equitable connectivity to essential service facilities (ESFs) during or after disasters. Their methodology incorporates factors such as population distribution, flood probability, topological importance (via minimal cut sets), and demographic characteristics. Links are evaluated individually, while paths are assessed by aggregating the ranks of their constituent links. Liu et al. (2018) adopted Multiattribute Utility Theory (MAUT) to evaluate scour-critical bridges through a sustainability-informed framework that integrates environmental, social, and economic dimensions. Their approach includes probabilistic failure analysis and quantifies consequences such as travel time delays, potential fatalities, and CO_2 emissions. Kopiika et al. (2025) developed a resilience-sustainability framework for post-conflict bridge recovery, explicitly addressing blast vulnerability, damage likelihood, and socio-economic significance. This framework is distinct in its focus on the challenges specific to human-induced damage in conflict zones, which differ from those in natural disaster contexts. Bhattacharjee and Baker (2023) proposed a sensitivity analysis-based method for prioritizing bridge retrofits in seismically vulnerable areas. Their approach uses global variance-based sensitivity analysis with total-order Sobol' indices to probabilistically rank bridges according to their influence on expected network disruption costs, capturing both individual and interaction effects across the network. Tran et al. (2024) examined the economic consequences of bridge closures by employing an expected consequence costing model. Their method quantifies detour-related losses and incorporates the costs associated with delays in emergency services, including ambulance, police, and fire response, as well as vehicle operating costs, accident risk, emissions, pavement wear, and freight delivery delays.

To overcome the limitations of purely topological metrics in capturing real-world traffic behavior, many researchers have adopted simulation-based methods. These approaches incorporate traffic assignment models and dynamic network conditions to provide more realistic representations of disruptions, such as bridge failures or road blockages, impact travel patterns, system performance, and overall network resilience. For example, Aghababaei et al. (2021) introduced the Trip Resilience (TR) metric, which evaluates robustness, redundancy, and recovery using traffic simulation under seismic failure scenarios. Their framework estimates changes in travel time and flow redistribution to generate a network-wide resilience profile. Wu et al. (2021) proposed a Level-of-Performance (LOP) framework for post-earthquake bridge network assessment, integrating Monte Carlo simulation, Latin Hypercube Sampling, and microscopic traffic simulation. Their methodology evaluates long-term restoration priorities by considering both traffic efficiency (travel time) and safety (predicted crash frequency in work zones), while accounting for uncertainties in seismic intensity and bridge fragility. Extending this line of inquiry, Gauthier et al. (2018) applied a stress-testing approach combined with a dynamic mesoscopic traffic simulator to assess network vulnerability. They quantified disruptions through increases in total travel cost and compared simulation-based rankings with those derived from topological metrics such as betweenness centrality. Their findings highlighted that disregarding traffic demand and congestion leads to misleading assessments, emphasizing the necessity of demand-responsive modeling.

Overall, simulation-based methods offer a powerful means to capture the cascading and temporal effects of network disruptions, model user behavior, and support informed prioritization of interventions. However, microscopic and mesoscopic simulations are computationally intensive and time-consuming, especially in large-scale or congested urban road networks. Additionally, these models require careful calibration and validation before they can be reliably used for analysis.

To mitigate the computational challenges associated with traffic simulations, researchers have increasingly turned to surrogate modeling techniques that approximate simulation outcomes with significantly lower computational demands. Silva-Lopez and Baker (2022) proposed the Corridors-Supported Optimization framework, which integrates neural networks and stochastic optimization to support bridge retrofitting decisions under seismic risk. Their approach identifies critical transportation corridors using a Markov Clustering Algorithm and jointly optimizes both pre-event retrofitting and post-event repair strategies to minimize expected travel time increases. Similarly, Li et al. (2024) developed a surrogate model based on random forests to predict traffic impacts resulting from bridge failures. Their method employs biased Markov random walks to estimate traffic flows and uses random forest regression to forecast average travel times, achieving a 98 % reduction in computational time compared to traditional agent-based simulations. Additionally, they introduced a comprehensive bridge ranking strategy that integrates One-at-a-Time (OAT) sensitivity analysis, Sobol' indices, and Gini importance measures, effectively capturing both local and global effects on traffic performance.

Despite considerable advancements in the identification and prioritization of critical links (e.g., bridges) for both pre-incident preparedness, such as retrofitting prioritization for seismic and flood-induced events, and post-disaster recovery, several research gaps remain. First, the majority of existing studies focus on seismic hazards, with relatively limited attention to developing generalized and simplified frameworks that consider all types of disruptions, including flood-related events, which are becoming increasingly relevant due to climate change. Second, purely topological methods, although computationally efficient, are less effective for capturing the wide effects of disruptions, as they neglect traffic demand, flow redistribution, and congestion effects, which are essential for realistic network performance assessment. Third, while simulation-based approaches provide more realistic assessments, they are

computationally intensive and time-consuming, which limits their scalability for regional or large-scale applications. Consequently, most studies have been restricted to small or localized networks. Finally, although surrogate models offer a promising solution by significantly reducing computational costs, they often require extensive, high-quality training datasets and resources that are not readily available in many regions. This limits their generalizability and practical adoption by transportation authorities and planners, especially in data-scarce or resource-limited contexts.

Building on these considerations, this study aims to address the identified research gaps by developing a network modeling methodology for the wide-area assessment of road network vulnerability to disruption events, with a particular focus on the prioritization of critical bridges. The proposed approach is intended to support transportation authorities and planners by enabling informed decision-making in response to disruption events at a regional scale, covering both urban and rural contexts. Designed for broad applicability, the methodology leverages publicly available online data and open-source software, including QGIS for geographic analysis and SUMO (Lopez et al., 2018) for macroscopic traffic simulation. By utilizing available data to estimate traffic demand, the iterative approach adopts a simplified incremental macroscopic route assignment combined with a quality indicator of the equilibrium condition to evaluate the reliability of the traffic flow distribution and the impacts of disruptions on network performance. The analysis first evaluates individual bridge-edge closures to identify their marginal effects and subsequently aggregates the results at the physical-bridge level and evaluates complete physical-bridge closures to support bridge-level prioritization. The applicability of the proposed framework is demonstrated through a case study in northern Italy, focusing on the Alessandria province in the Piedmont region under flooding scenarios.

The paper is structured as follows: Section 2 outlines the methodology and framework of the study, Section 3 introduces the study area along with the data used for the analysis; Section 4 presents the comparison between SUE and incremental assignment in the baseline scenario; Section 5 presents the results of the bridge criticality assessment, including the edge-based analysis, physical-bridge closure analysis, comparison with a topological ranking, and traffic-demand sensitivity analysis; and Section 6 concludes the paper with recommendations for future research.

2. Methodology

Following the objectives of this study and the insights gained from the literature review, a simplified incremental macroscopic simulation-based approach is adopted to estimate traffic flow redistribution across the road network and to identify the most critical bridge edges and physical bridges in a large-scale regional road network under disruption scenarios. Rapelli et al. (2019, 2022) conducted traffic flow simulation on a large-scale road network in the metropolitan area of Turin, Italy. Their findings demonstrated that modeling such a large-scale network is feasible with minor simplifications while still achieving an acceptable level of reliability. They also showed that macroscopic traffic assignment approach is effective in estimating link-level traffic flows on large road networks.

Compared to microscopic simulation methods, the macroscopic approach is faster, requires significantly less computational effort, and demands fewer data inputs. It is also more easily replicable and adaptable to different regional contexts, particularly given the increasing availability of open-source geographic data, including detailed road attributes. Macroscopic traffic assignment seeks to approximate the results of microscopic simulations in a more computationally efficient manner (Lopez et al., 2018). Instead of simulating individual vehicle movements at each time step, it uses mathematical functions to estimate travel time increments due to congestion.

In SUMO, this is implemented via the marouter tool (SUMO, Marouter), which employs a set of capacity-constraint functions to compute travel times and traffic flows based on parameters such as speed limits, number of lanes, and edge priorities. Each edge is assigned a priority level, which determines the per-lane capacity. The total capacity of an edge is then calculated by multiplying the per-lane capacity by the number of lanes. Although it is less detailed than microscopic and mesoscopic approaches, since travel times are estimated at the link level for aggregated flows rather than measured for each simulated vehicle, the method has been shown to produce results consistent with expectations in various case studies (Tsapakis et al., 2013; Balijepalli and Oppong, 2014; Zhu et al., 2021).

Although SUMO is primarily designed for microscopic and mesoscopic simulations, the same data structure for the road network can also be used for macroscopic traffic flow assignments. The marouter tool performs macroscopic traffic assignment, distributing traffic flows across available routes using inputs such as origin–destination (O–D) matrices and trip files. The output includes flow data with fully specified routes and associated probabilities, which can also be used as input for microscopic or mesoscopic simulations, thereby facilitating a multi-scale traffic analysis framework. It supports two traffic assignment algorithms: Stochastic User Equilibrium (SUE) and Incremental assignment.

The SUE model distributes traffic such that no driver can unilaterally reduce their travel time by changing routes, while also accounting for stochastic variations in route choice behavior. In SUE, users are assumed to perceive travel costs with random variations that can be modeled by different distributions. In the multinomial logit model, which represents the simplest form of random utility theory, the unexplained portion of perceived cost is assumed to follow an independent and identically distributed Gumbel (Type-I Extreme Value) random variable with zero mean and scale parameter Θ. This parameter controls the degree of sensitivity to travel time differences: smaller Θ values imply greater randomness in route choice, whereas larger Θ values lead users to increasingly favor the shortest path (more deterministic route choice). The input for this route choice method is a weight or cost function (W) on the network edges, coming from the simulation or default costs, and a set of routes R, where each route r has a cost C_r and a probability P_r. At each iteration, a new cost C'_r is estimated based on congestion effects modeled through the cost functions, and a new probability P'_r is assigned. The Logit mechanism applies a fixed formula to each route to calculate the new probabilities. For each route r, the new cost is

computed as the sum of edge costs Eq. (1) and route choice probabilities are then updated using the logit expression Eq. (2) (SUMO, Marouter [WWW Document], 2025; SUMO, Dynamic User Assignment [WWW Document], 2025):

$$C'_r = \sum_{e \in r} W(e) \tag{1}$$

$$P'_r = \frac{exp(-\theta C'_r)}{\sum_{s \in R} exp(-\theta C'_s)} \tag{2}$$

To evaluate the impact of the dispersion parameter on convergence and route-choice stability, multiple Θ values (default value is 0.01) are tested in this study:

Θ = 0.001, 0.0025, 0.005, 0.0075, 0.01, 0.025, 0.05, 0.075, 0.1.

The SUE algorithm operates with nested loops, an outer loop for generating new routes and an inner loop for computing probabilistic user equilibrium. In this study, the maximum number of outer iterations is set to 20, and the number of inner equilibrium iterations to 1000. All simulations employed a fixed convergence tolerance for SUE stability between consecutive solutions during the iterative process (tolerance = 0.001). Following Cascetta (2009), chapter 3, for each Θ-level, the implied variance of perceived travel costs is derived from the Gumbel distribution associated with the logit model. A coefficient of variation (CV) is then computed to quantify the relative level of randomness for each Θ. These variance and CV values are presented in section 4 to interpret how stochasticity influences the equilibrium solution.

An approximate but computationally efficient alternative is the incremental assignment method, which iteratively allocates fractions of the demand according to updated network conditions. In each iteration, a percentage of demand is assigned using the travel times obtained from the previous iteration. The main strength of incremental assignment is its high processing efficiency, which is substantially faster than SUE, an important advantage when testing many disruption scenarios within limited computation time. For this reason, incremental assignment is adopted as the primary method in this study, as it provides a fast and sufficiently reliable estimation of traffic flows suitable for large-scale networks and scenario-based analyses. The Dijkstra algorithm is used to compute the fastest routes. For each O–D pair, up to five alternative routes are allowed, and assignments are performed for a one-hour simulation window (0–3600 s), corresponding to the morning peak period.

It should be noted that the retained alternatives do not necessarily represent fully independent routes. In marouter algorithm, additional paths are generated through a penalty-based procedure, in which edges belonging to previously identified shortest paths are penalized before recalculating subsequent routes. Therefore, the number of alternatives represents an upper bound, and fewer distinct routes may be generated when sufficiently different paths are not available. In SUE with logit-based route choice, the overlap among alternative paths can be partially controlled through model parameters (e.g., commonality-related terms), allowing a more refined representation of route choice behavior when multiple similar alternatives exist. However, these approaches are computationally more demanding, particularly for large-scale networks. In contrast, in the incremental assignment adopted in this study, no explicit parameter is used to control the overlap among routes. Alternative paths are effectively activated only when congestion increases the cost of the current minimum-cost path, making detours competitive with respect to the minimum. Therefore, the emergence and use of alternative routes depend on network conditions rather than being imposed on an overlapping condition.

To evaluate the quality of the macroscopic assignment solution and assess its effectiveness, particularly when employing the incremental assignment method, an indicator, Delta (δ), is used (de Dios Ortuzar and Willumsen, 2011). This metric quantifies the degree to which the traffic flow solution approaches User Equilibrium (UE), in accordance with Wardrop's first principle, which states that no traveller can reduce their travel cost by unilaterally changing routes. It is defined as:

$$\delta = \frac{\sum_{ijr} T_{ijr}(C_{ijr} - C^*_{ij})}{\sum_{ij} T_{ijr} C^*_{ij}} \tag{3}$$

where T_{ijr} is the number of trips between origin i and destination j using route r; C_{ijr} is the cost (e.g., travel time) of route r; and C^*_{ij} is the minimum travel cost for the O–D pair (i, j) across all available routes. This indicator measures the total excess travel cost incurred by users selecting suboptimal routes, normalized by the total cost under optimal routing. A lower δ value indicates a solution that is closer to equilibrium, with less deviation from the most efficient travel paths. All cost values are computed after the final iteration of the assignment process once the traffic flows have stabilized across the network.

The assignment process uses the trips stored in the O–D matrices to estimate the distribution of traffic between traffic assignment zones (TAZs) over the available routes. The resulting traffic flows represent a macroscopic-level approximation of demand and can be visualized on the map at both link and route levels. Further analysis of the assignment results can be conducted using the network load output, which provides key traffic indicators at defined time intervals for each edge in the network. These indicators include the average travel time required to cross an edge, accounting for congestion and the assigned traffic flow; the average speed on an edge, calculated using travel time and edge length; the number of vehicles entering each edge during a specified time interval; and the flow-capacity ratio, representing the percentage of the edge's total capacity utilized by the assigned traffic flow. These outputs enable temporal analysis of traffic flow dynamics and facilitate the identification of congestion patterns and critical road segments.

2.1. Definition of study area and zones

The first step in the analysis involves defining the geographical extent of the study area, based on the scope of the assessment. The

use of open-source geospatial data, such as vector shapefiles containing administrative boundaries of provinces and municipalities, can support this phase. Depending on the type of disruption considered, hazard maps may also play a key role. In this study, shapefiles representing river catchment areas within the region of interest are employed to delineate the study area based on hydrological characteristics and rainfall patterns. Floodplain maps, providing information on flood return periods and the severity of potential flood events, are essential for identifying flood-prone areas and for generating static flood scenarios. These datasets, including administrative boundaries and flood hazard layers, are typically available through official geoportals or online sources such as OpenStreetMap (OSM).

Once the study area is defined, it is subdivided into traffic analysis zones (TAZs). Administrative boundaries, typically at the municipal level, are adopted as the basis of defining these zones, which include attributes such as name, code, area, and population. Based on the defined study area and its internal TAZs, external zones may also be introduced to accurately model and simulate external and crossing trips. This requires identifying some key entry and exit points along the perimeter of the study area. The main roads traversing the study area, including motorways and several national roads, can be identified as important access points that serve as external connectors to the regional network.

2.2. Road network model

The road network model is developed by selecting relevant road elements from the existing transportation infrastructure. A dataset containing attributes such road type, classification, edge length, number of lanes, traffic direction, and speed limits is utilized to support the modeling process. Additional data on critical infrastructure components, such as tunnels, viaducts, and bridges, are integrated to facilitate vulnerability assessments under disruption scenarios. Key shapefiles and datasets, including the road network, are typically sourced from official geoportals or open-access platforms such as OpenStreetMap (OSM).

Following the preparation of the road network model and zoning data, the final TAZ file (taz.xml format) is generated using the edgesInDistricts.py script. This tool parses the road network (net.xml format) along with a list of polygonal zones (typically shapefiles representing administrative or custom-defined boundaries) and generates a TAZ file that assigns each road edge to its respective zone. The script requires that the input TAZ polygons use the same coordinate reference system as the road network data to ensure spatial consistency. The resulting TAZ file contains zones identified by their unique IDs, corresponding to the input polygons. Each TAZ includes the road edges located within its boundaries, which are classified as sources or sinks for traffic generation and attraction. The weight of each edge within a TAZ is calculated based on its length and the number of lanes. The use of edge-based weighting for trip generation and attraction aims to distribute demand across the network within each TAZ, avoiding the concentration effects typically associated with centroid-based connectors. This approach provides a more spatially distributed representation of trip origins and destinations within the edges of the TAZs and allows the inclusion of intrazonal trips in the simulation, while maintaining a simplified and scalable demand modeling framework (Charlang Bakhtyari et al., 2025). This is particularly relevant in congested networks, where centroid-based connectors may introduce artificial concentration of flows and local saturation phenomena (Jafari et al., 2015).

2.3. Traffic demand

Next step in the analysis involves integrating traffic demand into the macroscopic traffic simulation. This requires datasets containing spatial and quantitative information on trip patterns, including:

- **Internal trips**: trips that originate and terminate within the study area.
- **External trips**: trips that start or end outside the study area.
- **Crossing trips**: trips that pass through the study area without originating or terminating within it.

Traffic demand data is typically derived from two main open data sources:

- **Mobility data from national census surveys**, which provide detailed insights into internal and external commuting trips.
- **Aggregated traffic flow data from motorways**, which are used to estimate crossing traffic demand.

Once the demand data is acquired, it is processed and incorporated into the simulation through a series of steps. Internal and external commuting trips, classified as internal–internal, internal–external, and external–internal trips, are generated using the randomTrips.py module, guided by the spatial distribution patterns derived from mobility data obtained from national census surveys. This module synthetically creates traffic demand by randomly selecting O–D pairs across the road network, either using a uniform distribution or a weighted probability distribution informed by the demand dataset. This probabilistic approach ensures that trip origins and destinations are spatially distributed across the network within each TAZ, rather than concentrated at specific nodes. The generated trips reflect typical commuting patterns within and across municipal boundaries in the study area. In parallel, motorway traffic flow, primarily representing crossing trips, is estimated based on aggregated traffic flow data from motorways. This dataset provides vehicle volumes along motorways, which are translated into direct trips between some entry and exit points on the motorway network. These flows are treated as direct links between predefined origin and destination edges, representing through traffic not captured by census-based commuting data (Charlang Bakhtyari et al., 2025). The synthetic weighted random commuting trips and motorway-based traffic flows are then merged to create a unified demand file (rou.xml format).

To convert these trips into a format suitable for macroscopic traffic assignment, the route2OD.py module is employed. This tool

generates an O–D matrix in the form of a TAZ-relation file by mapping each trip's start and end edges to their corresponding traffic analysis zones, based on a pre-defined TAZ file. The resulting O–D matrix represents aggregate demand between TAZ pairs to be used as input for macroscopic route assignments.

2.4. Disruption scenario

As indicated in the aim of this study, the focus is on flood-related disruption events. Based on the reviewed literature, flood disruption scenarios can generally be classified into two main types:

- **Static flood scenarios**: These are created by overlaying floodplain maps with the road network to identify infrastructure elements, particularly bridges, located within flood-prone areas. Once identified, these affected bridge edges are removed from the simulation to emulate real-world closures during or after flood events.
- **Dynamic flood scenarios**: These require more detailed datasets, including temporal rainfall records and a Digital Elevation Model (DEM), to simulate the evolving spatial and temporal characteristics of flood events. Such models enable the assessment of progressive impacts of flooding on traffic over time (Shahdani et al., 2022).

Due to limitations in the available data, this study adopts static flood scenarios to simulate flood-induced disruptions. Bridge edges exposed to flooding are identified by spatially intersecting the road network with floodplain maps. These identified links are then excluded from the road network model prior to macroscopic traffic simulation to represent the loss of connection caused by flooding.

In this study, the primary disruption scenarios are implemented by closing one bridge edge at a time, assuming independent edge failures. This assumption provides a simplified but controlled framework to isolate the marginal impact of each bridge edge on overall network performance and to enable a consistent ranking of bridge-edge criticality, in line with one-at-a-time (OAT) approaches commonly adopted in critical infrastructure analysis, although these approaches are limited in capturing interaction effects among multiple failures (Li et al., 2024). It is acknowledged that, in real flood events, multiple bridges and road segments within the same floodplain may be simultaneously affected; however, the spatial extent and combination of affected links depend on event-specific factors such as rainfall intensity, basin morphology, and flood propagation dynamics, introducing significant uncertainty. Considering all possible multi-edge disruption combinations would substantially increase computational complexity and reduce the scalability of the approach for wide-area networks. Moreover, simultaneous closures would quantify the combined impact of a specific disruption scenario rather than isolate the marginal contribution of each bridge needed for consistent bridge prioritization. To complement the edge-based analysis, edges representing the same physical bridge are also grouped and closed simultaneously to evaluate the disruption associated with the complete closure of the structure. This bridge-level analysis provides a representation of physical bridge failure and enables comparison with the criticality patterns obtained from individual edge closures. Nevertheless, the methodology can be extended to simultaneous multi-bridge disruption scenarios by defining a post-event condition and progressively restoring bridges to evaluate their contribution to network recovery. Such analyses would require the edges belonging to each physical bridge to be treated jointly, together with event-specific flood information identifying the bridges simultaneously affected and their restoration sequence. In addition, flood impacts may also involve partial capacity reductions (e.g., speed reductions due to water depth), which are not explicitly modeled in the present study. To iteratively simulate the disruption scenarios, a custom Python script was developed to systematically modify the "allow" attribute of selected edges, effectively disallowing all vehicle types on those links in the road network file. For the edge-based analysis, each selected bridge edge is closed individually, whereas for the physical-bridge analysis, all edges associated with the same physical bridge are closed simultaneously. This process enabled the automatic generation of a sequence of disrupted road network configurations for subsequent macroscopic traffic assignment. However, regardless of the type of disruption, the proposed methodology can also be applied to other hazard scenarios to evaluate their impact on overall road network performance.

2.5. Evaluation and sensitivity analysis

After developing the baseline and disrupted road networks configurations, the marouter tool is used iteratively to simulate each scenario and assign traffic demand (O–D matrix) to the road network. A constant demand assumption is adopted throughout the analysis, meaning that travelers were assumed to maintain their travel behavior and mode choice regardless of the flooding conditions. Under this assumption, the simulations evaluate how the existing travel demand within the study area can be accommodated when specific bridge closures occur. The simulation aimed at:

- Assessing how bridge-edge and physical-bridge closures affect the overall network vulnerability.
- Identifying the most critical bridge edges and physical bridges.
- Determining the most significantly impacted O–D pairs.

To facilitate this process, a custom Python script was developed to automate the macroscopic traffic assignment for each road network scenario employing the incremental assignment method. This allowed for the systematic simulation of the considered bridge closure scenarios, with corresponding outputs stored for further analysis. The key outputs generated from each simulation include:

- **Route Probability:** Indicating the probability of distribution of route choices between O–D pairs under each disruption scenario.

- **Network Load (netload):** Providing traffic flow metrics for individual road segments, enabling a quantitative evaluation of the impact of bridge closures on network performance.

To assess the vulnerability of the road network under different bridge closures and identify the most affected O–D pairs, a Weighted Time (WT) indicator is introduced. This indicator calculates the weighted average travel time for each O–D pair as follows:

$$WT_{ij} = \frac{\sum_{k=1}^{n} P_k C_k}{\sum_{k=1}^{n} P_k} \tag{4}$$

where WT_{ij} is the weighted time for the flow between the O–D pair (i, j); P_k is the probability of route k between the O–D pair; C_k is the cost (travel time) of route k; and n is the total number of available routes between the O–D pair.

To quantify the impact of bridge disruptions, the weighted time in each disrupted scenario is compared against the baseline scenario using both absolute and relative differences:

$$DifferenceWeightedTime(DWT_{ij}) = WT_{ij.Disrupted} - WT_{ij.Baseline} \tag{5}$$

$$PercentageDifferenceWeightedTime(\%) = \frac{WT_{ij.Disrupted} - WT_{ij.Baseline}}{WT_{ij.Baseline}} * 100 \tag{6}$$

To incorporate travel demand into the analysis, the difference weighted time is multiplied by the number of trips between O–D pairs, resulting in a demand-sensitive measure of network vulnerability:

$$DifferenceWeightedTimewithDemand = DWT_{ij} * T_{ij} \tag{7}$$

Where T_{ij} is the number of trips between the O–D pair (i, j).

Finally, additional network performance indicators are derived from the netload files, which constituted the second output of the

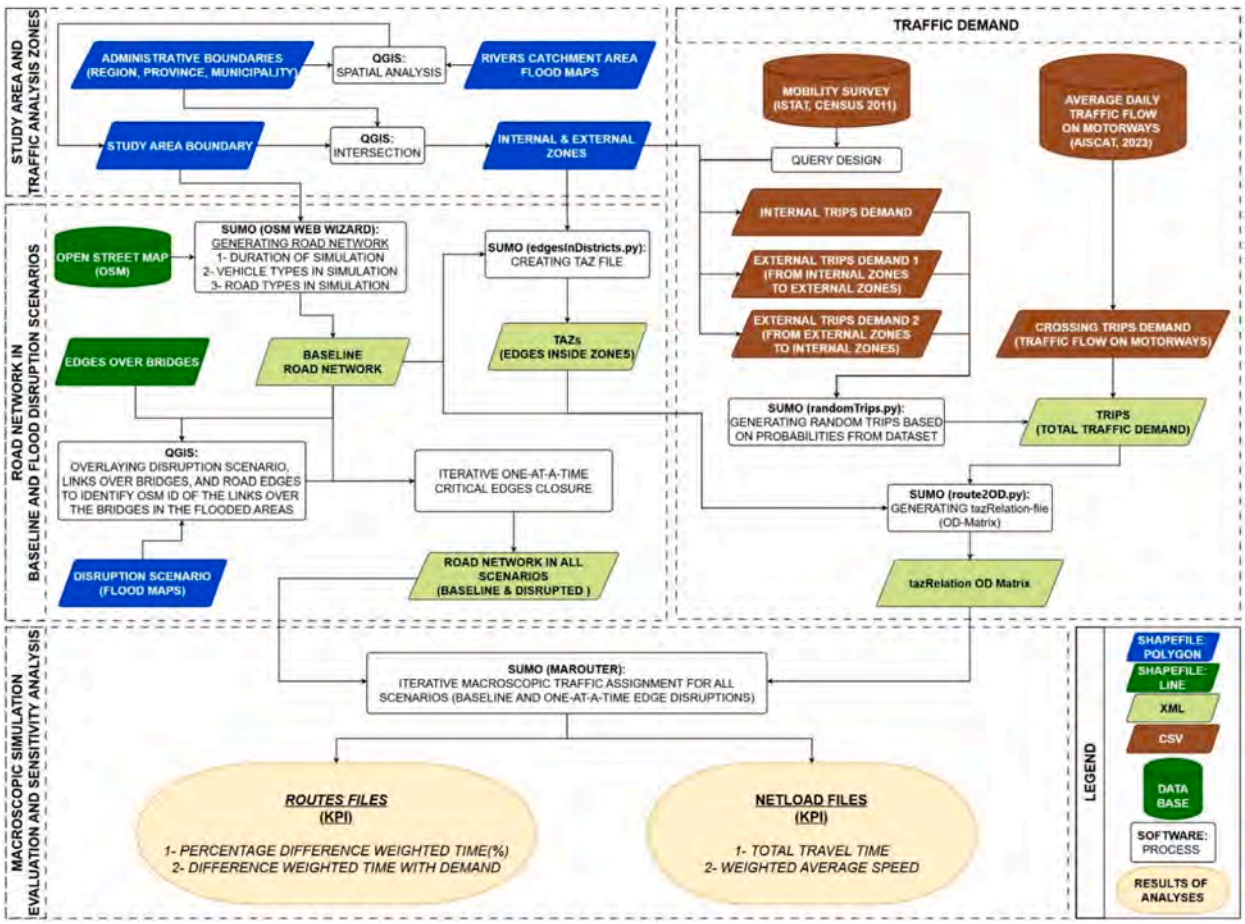

Fig. 1. Framework for identifying critical bridges based on iterative incremental macroscopic traffic simulation.

macroscopic simulation. These indicators offer an understanding of the network's behaviour under different disruption scenarios:

- Weighted Average Speed: This indicator evaluates the average speed across the network, accounting for both the duration associated with each edge and the number of vehicles using it. It is computed as:

$$WeightedAverageSpeed = \frac{\sum_{Edge=1}^{n}(TravelTime_{Edge}*Entered_{Edge}*Speed_{Edge})}{\int_{Edge=1}^{n}(TravelTime_{Edge}*Entered_{Edge})} \tag{8}$$

where travel time represents the average travel time on each edge, speed is the average speed on each edge, and entered is the number of vehicles that entered each edge during the considered time interval.

- Total Travel Time: This represents the cumulative time spent by all vehicles across the entire road network and is calculated as:

$$TotalTravelTime = \sum_{Edge=1}^{n}(TravelTime_{Edge}*Entered_{Edge}) \tag{9}$$

- Total Travel Distance: This represents the cumulative distance travelled by all vehicles across the entire road network and is calculated as:

$$TotalTravelDistance = \sum_{Edge=1}^{n}(Length_{Edge}*Entered_{Edge}) \tag{10}$$

Fig. 1 presents an overview of the proposed quantitative framework for the identification of critical bridges.

3. Case study and materials

The study area, traffic analysis zones, baseline road network, the datasets used to estimate travel demand, and flood hazard data in this research are the same as those described in Charlang Bakhtyari et al. (2025); a short summary is provided here for completeness.

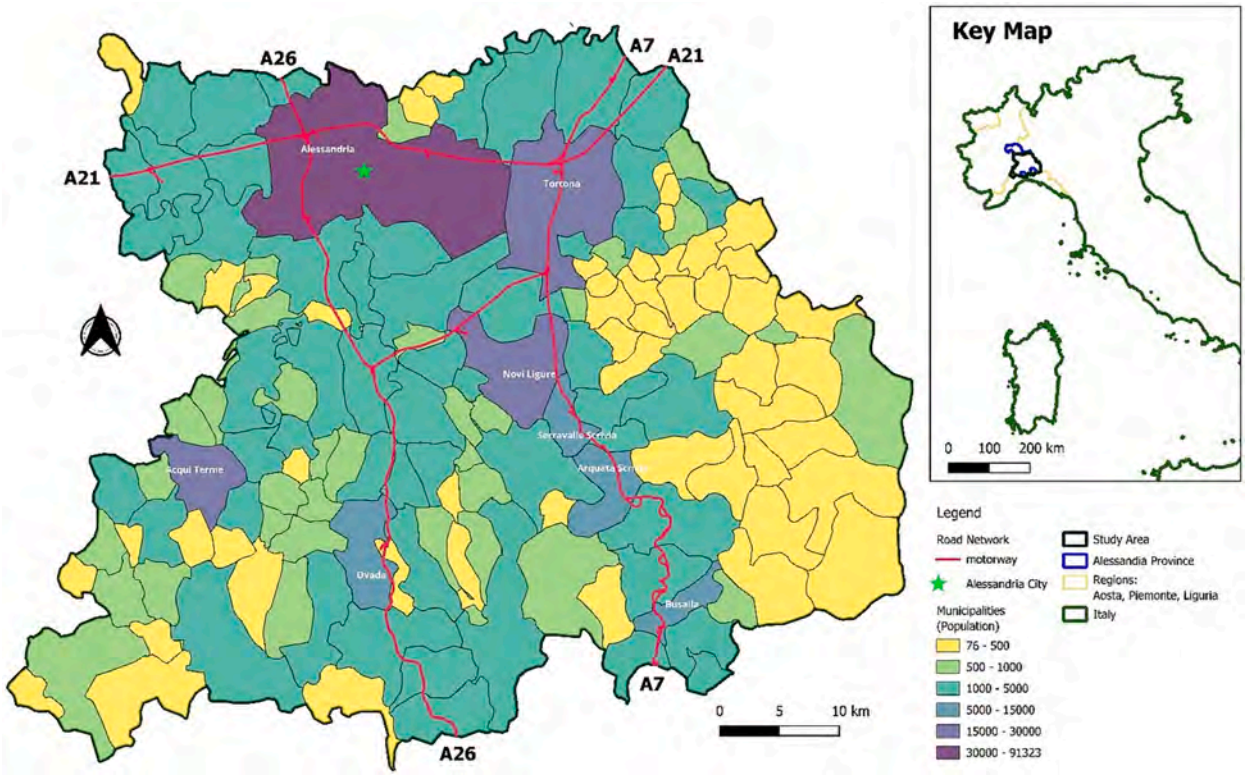

Fig. 2. Study area.

Certain additional processing and integration of these datasets were performed as required for the present study.

3.1. Study Area, TAZs, and baseline road network

The selected study area is located in northwestern Italy, specifically in the southern part of the Piedmont region. It encompasses the province of Alessandria along with selected adjacent municipalities in the Liguria region. In total, the study area consists of 146 municipalities, including 134 from the province of Alessandria and 12 from the Liguria region. The total population of the study area is approximately 342,964 inhabitants, covering an area of 3070.27 km^2. The municipality of Alessandria, with a population of 91,323, serves as the primary urban center within the region (Mandarino et al., 2021). Fig. 2 presents the study area, illustrating municipal boundaries, population distribution, and the regional motorway network. All shapefiles representing the study area and municipalities (Geoportal of Piedmont, Administrative areas [WWW Document], n.d) were obtained as publicly available datasets. All maps were created using the WGS 84 UTM Zone 32 N coordinate reference system and the Universal Transverse Mercator (UTM) projection.

To accurately model and simulate external and crossing traffic, it was necessary to define external zones and identify some key entry and exit points around the study area. The main roads traversing the study area, including motorways A21, A26, and A7, as well as several national roads, were identified as important access points. In total, 13 boundary points (road edges) were defined along the perimeter of the study area (Fig. 3). Additionally, one supplementary entry and exit point was designated within the study area to specifically model crossing trips on motorway A7. These points function as origins or destinations for external trips, connecting external zones with internal traffic analysis zones, and as entry and exit locations for vehicles traversing the study area without stopping.

To define the external zones, spatial data processing was conducted in QGIS using a shapefile of municipal boundaries across Italy (Istituto Nazionale di Statistica, Administrative areas [WWW Document], n.d). By overlaying this shapefile with the layer representing the entry and exit points of the study area, all municipalities outside the study area were classified as 13 external zones. These zones were then linked to the study area via the defined boundary points (Fig. 3). Table A. 1 in Appendix section lists the entry and exit points to the study area.

The road network dataset for macroscopic traffic simulation (net.xml format) was generated from OSM for the specified study area and road classifications (Fig. 4). For visualization purposes in Fig. 4, road edges are grouped into five categories (motorway, trunk, primary, secondary, and local). The 'local' category includes all lower-level road classes (e.g., tertiary, residential, living street, and unclassified), while in the simulation model each edge retains its original OSM classification. The resulting road network spans a total length of roughly 11,510 km and comprises 46,619 links and 20,850 nodes, accounting for multilane edges. In addition to geometric features, the dataset includes attributes such as edge length, the presence of bridges and tunnels, road names, speed limits, one-way restrictions, traffic direction, and access permissions, making it suitable for realistic traffic modeling and flood vulnerability analysis.

After preparing the road network model and zoning data, the final TAZ file (in taz.xml format) was generated using the

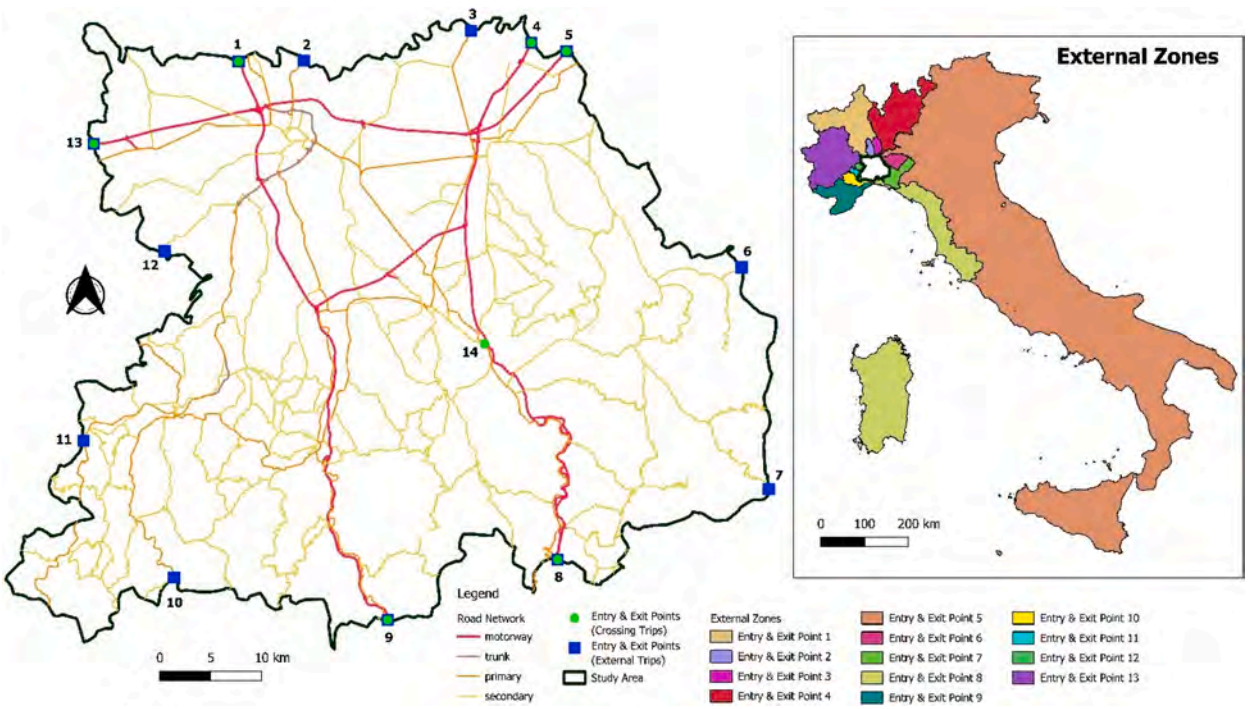

Fig. 3. External zones and entry and exit points.

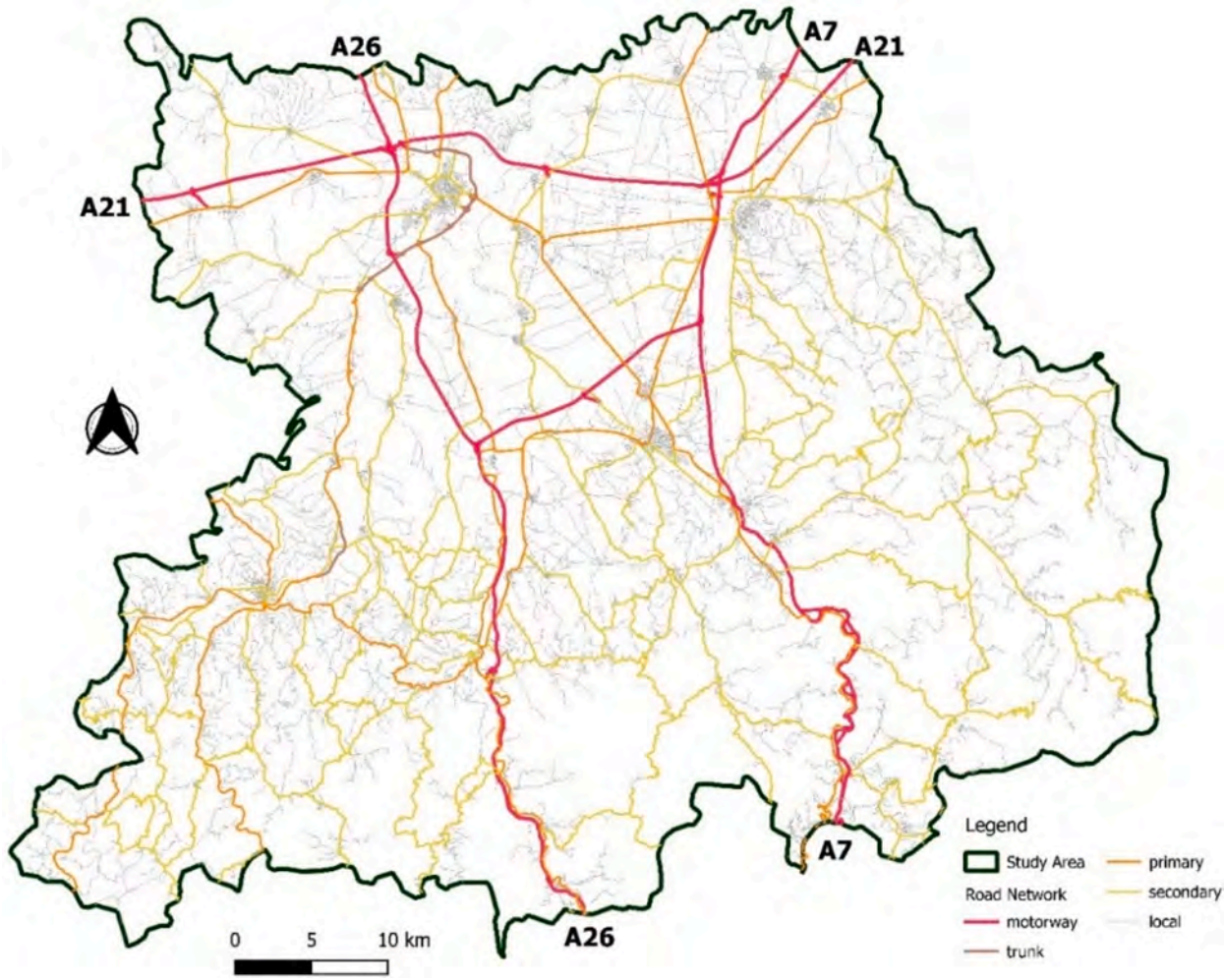

Fig. 4. Road network.

edgesInDistricts.py script. Each TAZ contains the road edges within its boundaries, classified as sources or sinks for traffic generation and attraction. For external zones, the boundary road edges of the study area serve as sources and sinks for both external and crossing trips.

3.2. Traffic demand data

To extract trip information and build the O–D matrix, two published Italian datasets were utilized (Charlang Bakhtyari et al., 2025):

- The ISTAT 2011 dataset provides an O–D matrix representing daily commuting movements for work or study purposes. It is derived from the 15th General Population Census, with a reference date of October 9, 2011 (Istituto Nazionale di Statistica, Commuting Matrices [WWW Document], n.d).
- The AISCAT 2023 dataset offers insights into aggregated traffic flow and accident statistics on Italian motorways (Associazione Italiana Società Concessionarie Autostrade e Trafori, Traffic flow on motorways [WWW Document], n.d).

Although these datasets refer to different time periods, their integration is intended to provide a representative approximation of demand for methodological application. The aim is to evaluate the proposed framework under realistic conditions rather than to reproduce a specific real-world traffic scenario in a given time period.

By querying the complete commuting matrix from ISTAT 2011, all trips originating and terminating within the 146 municipalities inside the study area were identified. The analysis focused on private vehicle trips, specifically those made by cars. Trip purposes were classified into two categories: home-based work (HBW) and home-based education (HBE). Additionally, the departure time was restricted to the morning rush hour period, between 07:15 and 08:15, to reflect peak commuter activity and ensure the highest rate of vehicle injection into the road network. This process yielded two probability tables indicating the likelihood of each internal TAZ

serving as an origin or destination for internal trips. Then, each edge in the network was assigned a probability of serving as either an origin or a destination according to the probability of the corresponding TAZ. These probability tables were then used to control the spatial distribution of origin and destination of trips during random internal trip generation. The adopted TAZ-based representation should be interpreted as a first-order approximation using available open datasets. While the zonal O–D totals are derived from observed census data, the spatial allocation of trips within each TAZ is probabilistically distributed across eligible edges to avoid concentration effects at single nodes. It is acknowledged that finer zoning systems, observed route choice behaviour, traffic counts, or calibrated demand datasets may modify the quantitative ranking of some bridge edges. Nevertheless, the proposed methodology does not exclude potential incorporation of higher-resolution demand inputs depending on data availability and research objectives.

In addition to internal trips, two layers of traffic demand were developed to represent external trips, combining both ISTAT 2011 data and the random trip generation method. Each external zone was associated with a predefined entry or exit point (Fig. 3). By linking external zone data with the external trip tables, each trip was assigned a specific boundary access point. Crossing trips were also incorporated, focusing on three major motorways (A21, A26, and A7) using average daily traffic flow data from the AISCAT 2023 dataset.

In total, the study accounted for 7245 internal trips, 2200 outbound external trips (from the study area to external zones), and 2200 inbound external trips (from external zones to the study area), all during the 07:15 to 08:15 peak period. Accordingly, random trip generation in the simulation was configured over a 3600-second (one-hour) interval. After merging the internal and external trips, an additional 9131 crossing trips along the motorways were added as direct flows between their respective entry and exit points. These combined layers formed the complete traffic demand dataset (rou.xml format) for the simulation. To aggregate traffic demand at a macroscopic level, the route2OD.py module was used to generate a TAZ-relation O–D matrix used as input for macroscopic traffic assignment.

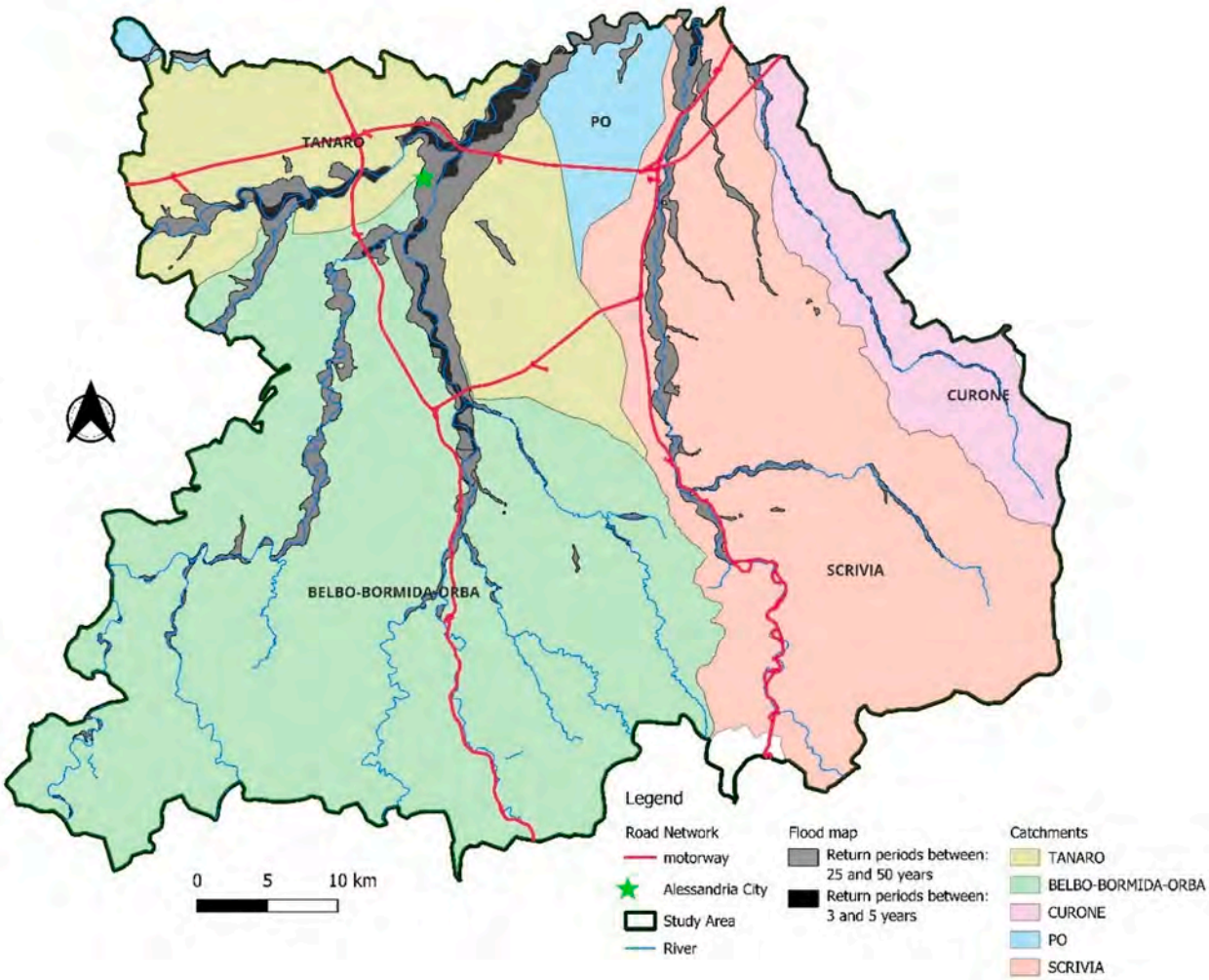

Fig. 5. Rivers, catchment areas, and floodplain map in the study area.

3.3. Floodplain map

The study area is intersected by several rivers with a known history of flooding, including the Tanaro, Bormida, Orba, and Scrivia rivers. Consequently, the area spans multiple hydrological catchments (Geoportal of Piedmont, Arpa Piemonte, Hydrographic basins [WWW Document], n.d): the Tanaro River in the northwest; the Belbo, Bormida, and Orba Rivers in the south and southwest; the Scrivia and Curone Rivers in the east and southeast; and the Po River in the north, as illustrated in Fig. 5. The flood hazard data used for disruption analysis was sourced from ARPA Piemonte (Regional Agency for Environmental Protection of Piedmont) and downloaded via the Geoportal of Piedmont (Geoportal of Piedmont, Arpa Piemonte, Floodable areas [WWW Document], n.d). The dataset provides a vector representation of flood-prone areas within the Piedmont region, including the Province of Alessandria, which serves as the study area. It classifies flood risk zones based on return periods and sediment types present in flooded areas (Fig. 5). These maps are derived from historical data, including documented flood events and aerial photograph analyses conducted up to the 1990 s. By integrating this flood hazard dataset with the road network model, the study aims to assess the vulnerability of critical infrastructure, particularly bridges, to flood disruptions. The resulting analysis may be used to support prioritization for retrofitting efforts, focusing on infrastructure elements whose failure would lead to significant network performance degradation under flood scenarios.

4. SUE vs. Incremental assignment in the baseline road network scenario

The finalized TAZ-relation traffic demand (O–D matrix) was applied to the baseline road network, and macroscopic simulations were conducted. This section compares the results of the two macroscopic traffic assignment methods introduced in Section 2: SUE with logit-based route choice and the incremental assignment method. Both methods were applied to the baseline road network scenario, allowing a direct assessment of their performance in terms of convergence, computational efficiency, and the distribution of traffic flows across the network. All simulations were performed on an Acer device with an Intel Core i7-7700HQ CPU running at 2.80 GHz, 16 GB of RAM (15.9 GB usable), a combination of 932 GB HDD and 119 GB SSD storage, and graphics provided by an NVIDIA GeForce GTX 1050 Ti (4 GB) alongside Intel HD Graphics 630 (128 MB). The system operates on a 64-bit architecture.

For the SUE method, different values of the dispersion parameter Θ were tested to evaluate its impact on convergence and route-choice stability. For each Θ level, the implied variance of perceived travel costs was derived from the Gumbel distribution associated with the logit model (Cascetta, 2009). A coefficient of variation was then computed to quantify the relative level of stochasticity for each Θ value. The standard deviation for the CV calculation was obtained from the variance, while the network-wide weighted mean travel time was calculated using the assigned flows and travel times across all O–D pairs. This allowed the CV to represent the relative dispersion in perceived travel costs. Additionally, the delta (δ) indicator, as defined in Eq (3), was calculated to quantify the closeness of the SUE solution to the deterministic User Equilibrium. The time required for each SUE simulation was also recorded to evaluate computational efficiency. Table 1 reports the results of SUE assignments for all tested Θ values, including the variance of perceived travel costs, the CV, the resulting delta value, and the total computation time required for convergence. As mentioned in Section 2, all simulations employed a fixed convergence tolerance for SUE stability. Therefore, differences in computation time can be attributed to the varying dispersion levels of route choice, as SUE converges to less restrictive equilibrium conditions compared to Deterministic User Equilibrium (DUE), which requires nearly identical travel times across alternative routes.

Subsequently, the macroscopic traffic assignment using the incremental method was performed on the baseline scenario. Table 2 presents the results of the incremental assignment, including the overall simulation duration and the final delta value obtained for the baseline scenario.

As shown in Table 1, the SUE assignment exhibits increasing route-choice dispersion for lower values of the logit sensitivity parameter Θ, with Delta values ranging from 0.12 % (near DUE) for $\Theta = 0.1$ to 7.90 % for $\Theta = 0.001$. Table 2 shows that the incremental assignment, although inherently a simplified and approximate method, achieves a Delta value of 1.85 %, which falls within the same range as the SUE results obtained for $\Theta \approx 0.005$–0.01. In this Θ range, the SUE model produces Delta values between 1.17 % and 2.38 %. However, the computational advantage of the incremental method is substantial: while the SUE runs for these Θ values require between 380 and 1087 s, the incremental assignment completes in only 51.72 s, nearly 20 times faster. This significant reduction in computation time makes incremental assignment particularly suitable for analyses requiring the evaluation of numerous disruption scenarios, such as testing the impacts of closing multiple bridges sequentially across a large-scale road network. Overall,

Table 1
Results of the SUE logit-based macroscopic traffic assignment for the baseline road network.

Theta (Θ)	Variance	SD	Mean Travel Time (sec)	CV (%)	Computation Time (sec)	Delta (%)
0.1	164.49	12.83	1783.87	0.72 %	6937.85	0.12 %
0.075	292.43	17.10	1783.22	0.96 %	4180.77	0.16 %
0.05	657.97	25.65	1782.62	1.44 %	3933.34	0.23 %
0.025	2631.89	51.30	1781.45	2.88 %	2548.13	0.47 %
0.01	16449.34	128.25	1784.66	7.19 %	1087.34	1.17 %
0.0075	29243.27	171.01	1785.48	9.58 %	705.23	1.59 %
0.005	65797.36	256.51	1788.04	14.35 %	380.66	2.38 %
0.0025	263189.45	513.02	1807.63	28.38 %	222.56	4.27 %
0.001	1644934.07	1282.55	1850.87	69.29 %	193.47	7.90 %

Table 2
Results of the incremental macroscopic traffic assignment for the baseline road network.

Mean Travel Time (sec)	Computation Time (sec)	Delta (%)
1790.37	51.72	1.85 %

these results confirm that the incremental assignment can achieve a reasonable balance between computational efficiency and solution quality, supporting its applicability despite potential overlaps among alternative routes.

5. Sensitivity analysis results and Discussion

For the disruption scenario analysis, the road network was overlaid with the floodplain map (Fig. 5 and Fig. 6) and the spatial distribution of bridges. Using a flood return period of 3–5 years, 12 physical bridge locations (Table A. 2 in Appendix section) were identified within flood-prone zones. Due to the representation of infrastructure in the OSM-based network, a single physical bridge may correspond to multiple road edges (e.g., directional links, ramps, or segmented geometries). Consequently, these 12 physical bridges corresponded to 52 affected road edges, which were selected for closure in the disruption scenarios. The initial analysis evaluated these 52 edges individually, while the subsequent physical-bridge analysis grouped the corresponding edges into the 12

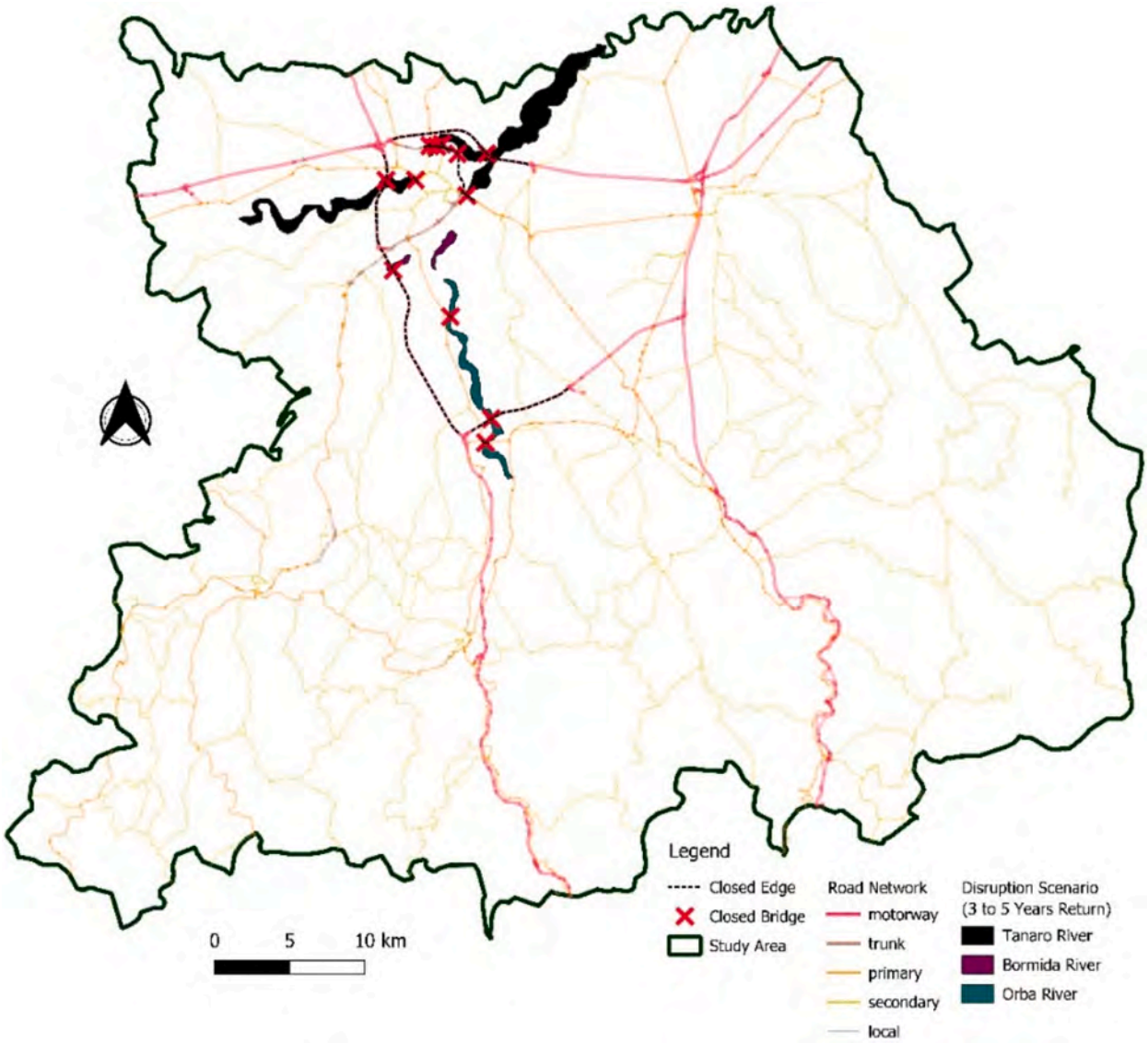

Fig. 6. Disruption scenario, closed bridges, and closed edges.

physical structures.

Fig. 6 illustrates the bridge locations and highlights the closed edges, each of which was closed individually in separate simulation runs. This process resulted in the creation of 52 modified road network files, each representing a network with one closed edge. These modified road network files (net.xml format), along with the baseline road network, the TAZ file, and the O–D matrix, were input into a custom Python script that automated the execution of incremental macroscopic traffic assignment for each road network configuration. The corresponding simulation results were stored for subsequent vulnerability analysis.

Following the methodology, the incremental traffic assignment was adopted for the case study, as it provides a computationally efficient and reasonably accurate solution for large-scale networks. Shortest paths were computed using the Dijkstra algorithm, with up to five alternative routes permitted for each O–D pair. Traffic assignment was performed over a one-hour simulation period (0–3600 s), representing the morning peak hour. The maximum number of iterations for updating route choices in the incremental user assignment was set to 20.

After running the incremental macroscopic simulation of the baseline and each disrupted road network scenario (with individual edge closures), two output files were generated per simulation: a route file and a network load file.

The route file includes detailed information on O–D traffic flows, such as the number of trips, departure and arrival times (consistent with the 0–3600 s simulation window), and the distribution of trips across available route alternatives. In addition, the file provides route-specific travel costs (times), route choice probabilities, and the sequence of OSM edge IDs that define each path.

A custom Python script was developed to process all route files associated with the baseline and disrupted scenarios. This script calculates the Delta (δ) value for each incremental macroscopic simulation. The Delta value quantitatively represents the deviation of each scenario from Wardrop's First Principle (User Equilibrium) as mentioned in section 2.5, thereby reflecting the extent to which disruptions affect overall traffic flows and route choices.

The computed Delta values across all scenarios are presented in Fig. 7. As illustrated, the Delta values remain within the range of 2–3 %, indicating that all simulations achieved a level of convergence exceeding 97 % with respect to equilibrium. This degree of convergence is considered acceptable for large-scale road networks, where slight deviations from perfect equilibrium are expected due to network size and complexity. These results provide a foundation for further evaluation of network performance using additional Key Performance Indicators (KPIs) and for gaining insights into the redistribution of traffic demand under various disruption scenarios.

5.1. Routes analysis

By further processing and analysing the route files, Table A. 3 in Appendix section presents a subset of O–D pairs for which the Percentage Difference Weighted Time Eq. (6)) exceeds 50 % in disrupted scenarios. Fig. 8 illustrates the maximum Percentage Difference Weighted Time observed across all scenarios, indicating severe disruptions in specific O–D pairs due to the simulated bridge-edge closures.

As shown in Fig. 8 and Table A. 3 in Appendix section, the most critical bridge edge is the one with OSM ID "-42259829", located over the Orba River in the central part of the study area. This closure results in a maximum Percentage Difference Weighted Time of 266 % for travel between zone 006,047 (Castellazzo Bormida) and zone 006,021 (Bosco Marengo). The adjacent bridge edge, with OSM ID "42259829", follows closely with a 233 % increase between zone 006,075 (Frugarolo) and zone 006,047 (Castellazzo

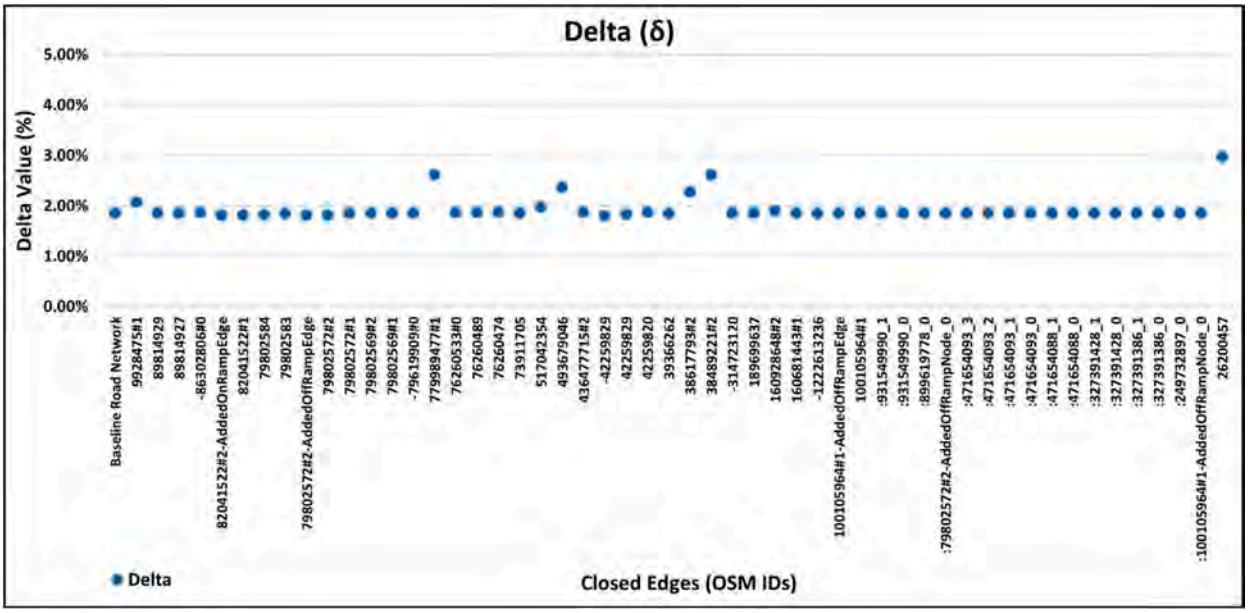

Fig. 7. Delta values.

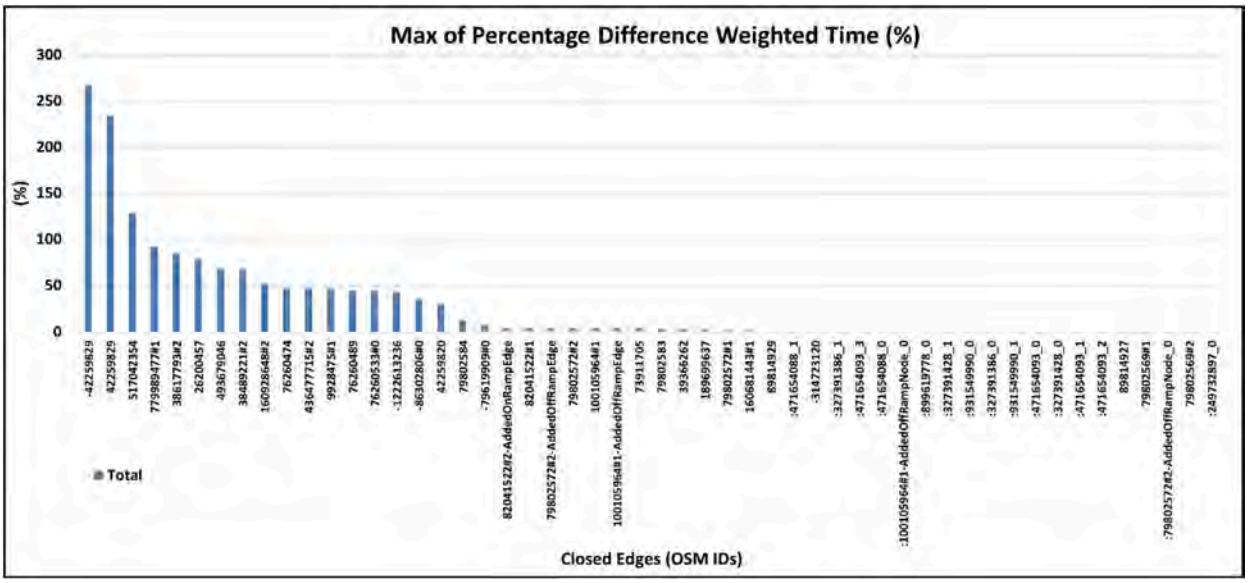

Fig. 8. Max of Percentage Difference Weighted Time.

Bormida).

While these edges show the highest increases in travel time, as illustrated in Fig. 9, they are located on local roads with relatively low traffic volumes. Therefore, incorporating trip demand into the analysis was crucial to accurately identify and prioritize critical bridge edges. This demand-sensitive approach ensures that priority is given to edges whose closures not only increase travel time but also significantly impact heavily used O–D pairs, thereby improving the network's overall capability to absorb traffic demand under disruption scenarios.

Table A. 4 in Appendix section presents a subset of O–D pairs for which the Difference Weighted Time with Demand Eq. (7) is notably high. Fig. 10 illustrates the maximum Difference Weighted Time with Demand observed across all disruption scenarios.

Considering traffic demand in the analysis and multiplying it to the Difference Weighted Time accordingly, Table A. 4 in Appendix section and Fig. 10 reveal that the most significant impact occurs when the bridge edge with OSM ID "26200457" is closed. This bridge edge, located on the A21 motorway connecting Torino (external zone 13) to Piacenza (external zone 5) over the Tanaro River, results in a total travel time increase of 1,026,110 s for 1111 vehicles during the one-hour simulation. The second highest impact is observed for the closure of edge with OSM ID "779989477#1", also on the A21 motorway (from Piacenza to Torino, crossing the Tanaro River), with a travel time difference of 975,389 s. Subsequent significant impacts are observed from the closure of edge with OSM ID "517042354" on the A26 motorway, which connects Gravellona (external zone 1) to Voltri (external zone 9) across the Tanaro River, and edge with OSM ID "9928475#1" (A26 motorway, from Voltri to Gravellona, crossing the Bormida River), both resulting in differences exceeding 800,000 s (Fig. 11).

This metric emphasizes that some bridge edges, despite having lower percentage differences weighted time, have a substantial absolute impact due to their high traffic volumes, particularly in crossing trips over motorways. As shown in Fig. 11, the indicator of Maximum Difference Weighted Time with Demand clearly identifies motorway bridge edges as the most critical, given their heavy vehicle loads and their function in facilitating internal, external, and cross-regional traffic flows between external zones.

5.2. Network loads analysis

The second output generated from the incremental macroscopic simulations is the network load file, which contains detailed edge-level information such as travel time, speed, entered flow, and flow capacity ratio. This data can be analyzed to evaluate the traffic dynamics of the road network under baseline and disrupted scenarios.

Fig. 12 illustrates the outcomes of this analysis, highlighting key network performance indicators, total travel time (veh.h), total travel distance (veh.km), and weighted average speed (km/h), across various bridge-edge closure scenarios. For the baseline scenario, the total travel time is 10,745 veh.h, the total travel distance is 669,399.7 veh.km, and the weighted average speed is 62.29 km/h.

The results derived from the network load file, as presented in Fig. 12, reveal variations in total travel time, total travel distance and weighted average speed, indicating that bridge closures lead to congestion and traffic rerouting. This analysis supports the identification of the most critical bridge edges across the study area.

- The highest total travel time was observed (Fig. 12 and Fig. 13) when the bridge edge with OSM ID "779989477#1" (A21 motorway, connecting Piacenza to Torino over the Tanaro River) was closed, reaching 11,272 veh.h, with a corresponding increase

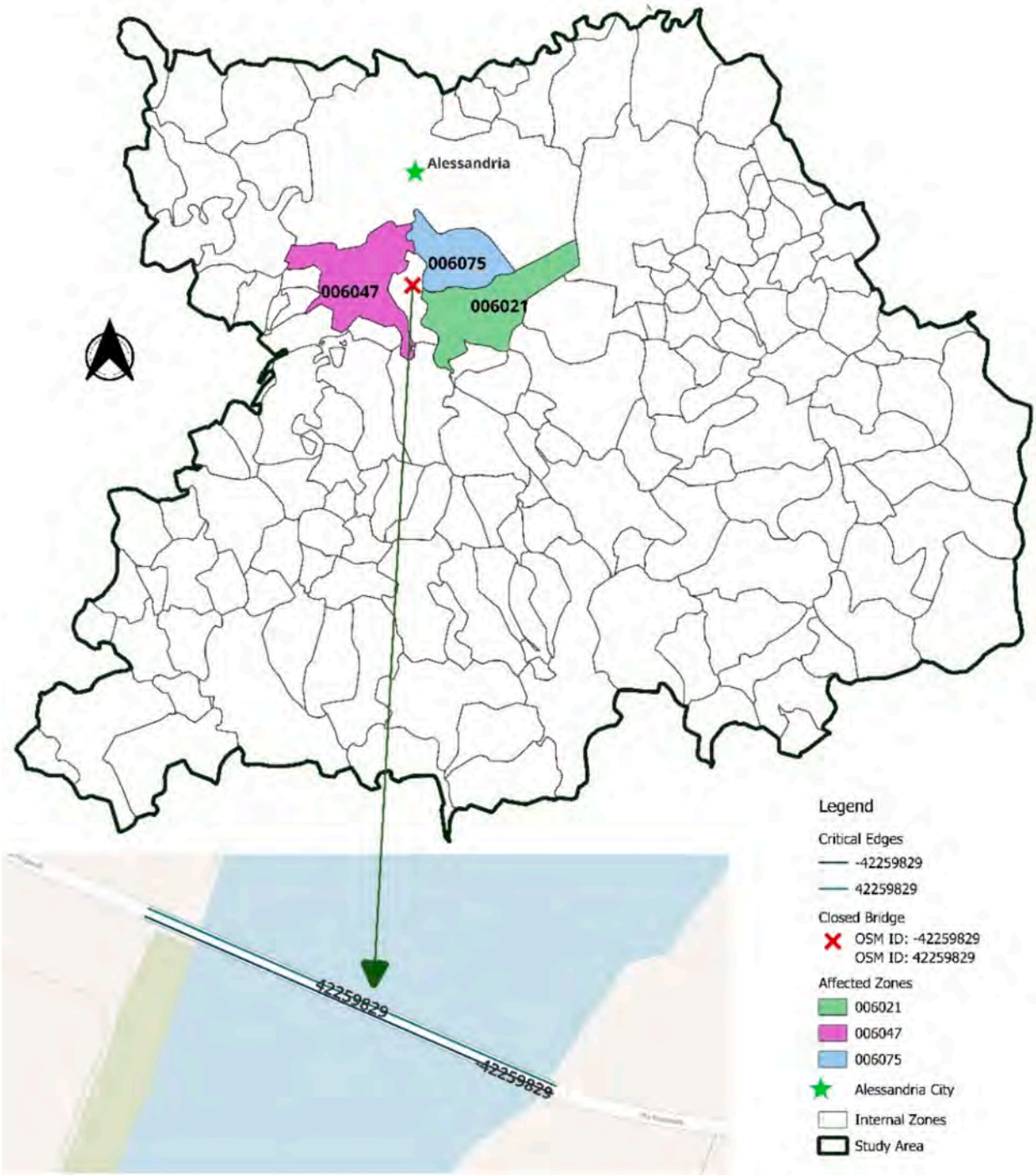

Fig. 9. Critical bridge edges (based on Max of Percentage Difference Weighted Time).

in total travel distance to 674,043.5 veh.km, and a decrease in weighted average speed to 59.79 km/h. This underlines the impact of this bridge-edge closure on overall network performance.

- Other critical bridge edges with significant increases in total travel time include (Fig. 12 and Fig. 13):
- Edge with OSM ID "9928475#1": total travel time = 11,237 veh.h; total travel distance = 673,694.4 veh.km; weighted average speed = 59.95 km/h (A26 motorway, connecting Voltri to Gravellona over the Bormida River).
- Edge with OSM ID "38489221#2": Total travel time = 11,232 veh.h; total travel distance = 676,406.9 veh.km; Weighted average speed = 60.22 km/h (A26 motorway, connecting Gravellona to Voltri over the Bormida River).

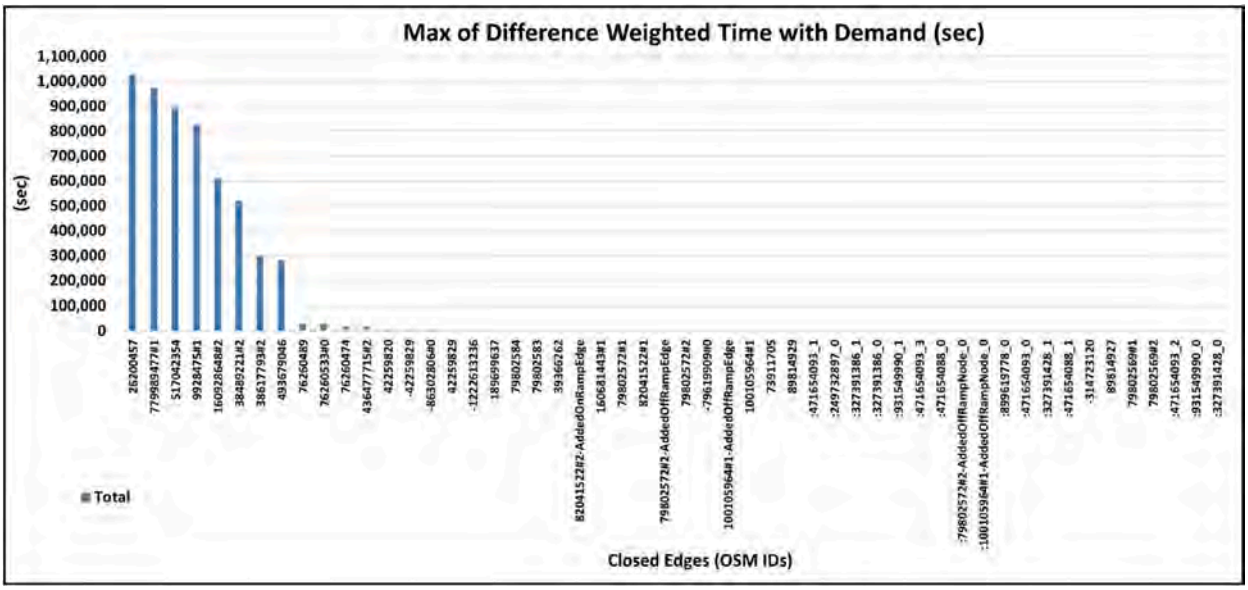

Fig. 10. Max of Difference Weighted Time with Demand.

- Edge with OSM ID "26200457": Total travel time = 11,115 veh.h; total travel distance = 673,484.7 veh.km; Weighted average speed = 60.59 km/h (A21 motorway, connecting Torino to Piacenza over the Tanaro River).

As seen in Fig. 12, in most cases where there is an increase in total travel time, there is also an increase in total travel distance, indicating the presence of longer detours due to bridge-edge closures. At the same time, a reduction in weighted average speed reflects congestion effects as a consequence of traffic redistribution. These cases represent the most severe disruptions, as the closures force users onto longer routes with lower speeds or overloaded alternative links, affecting both network geometry and capacity. However, as observed in the results of the route analysis, in all disruption scenarios all O–D pairs remain reachable through detours, indicating that the overall network connectivity is preserved. Furthermore, as shown in Fig. 12, the highest increase in total travel distance is associated with the bridge edge with OSM ID "38489221#2", with a total travel distance increase of just over 1 % (from 669,399.7 veh.km in the baseline scenario to 676,406.9 veh.km), suggesting that alternative routes in the network remain relatively efficient and that reasonable routes still exist between O–D pairs. As also illustrated in Fig. 12 and Fig. 13, for the bridge edge with OSM ID "493679046" (connection between motorways A26 and A7), total travel time increases and weighted average speed decreases compared to the baseline scenario, while total travel distance slightly decreases. This indicates that traffic is redistributed onto shorter but more congested routes, where lower speeds and capacity constraints lead to increased travel times despite reduced travel distances.

These findings demonstrate that increases in travel time are not solely driven by longer detours, but are also influenced by congestion and traffic redistribution effects. The combined analysis of total travel time, total travel distance, and weighted average speed enables a clearer interpretation of the underlying mechanisms of disruption, allowing the distinction between detour-driven impacts and congestion-driven effects, and thus providing a more comprehensive assessment of network vulnerability.

The findings based on the indicators employed in this study demonstrate that motorway bridge-edge closures result in substantial increases in travel time and cost. In particular, the Difference Weighted Time with Demand and Total Travel Time indicators provide strong evidence that closures along motorway bridges significantly disrupt traffic flows due to the high commuter volumes typically observed on these routes. These results show the critical role that motorway bridges play in maintaining connectivity in the study area and the importance of resilience strategies to ensure the operational reliability of key motorway bridges during disruption events such as floods, especially those crossing the Tanaro, Bormida, and Orba rivers. Moreover, while the Percentage Difference Weighted Time indicator is useful in capturing localized impacts of disruptions on travel costs, it does not account for traffic volumes and should therefore be interpreted as a complementary measure when prioritizing bridges for retrofitting or mitigation measures.

5.3. Physical-Bridge closure analysis

The preceding analyses evaluated the marginal impact of closing individual bridge edges. However, as illustrated in Fig. 6 and listed in Table A. 2, the 52 flood-exposed road edges correspond to 12 physical bridges. To translate the edge-level results into a form more directly applicable to bridge prioritization, the 52 bridge edges were therefore grouped according to their corresponding physical bridges. As a first step, the edge-based results were aggregated at the physical-bridge level. For each of the 12 bridges, the maximum Percentage Difference Weighted Time and maximum Difference Weighted Time with Demand obtained among its constituent edge-closure scenarios were retained. These indicators represent the greatest impact experienced by an individual O–D pair among the corresponding edge-closure scenarios, respectively in relative travel-time terms and in absolute demand-weighted terms. The resulting

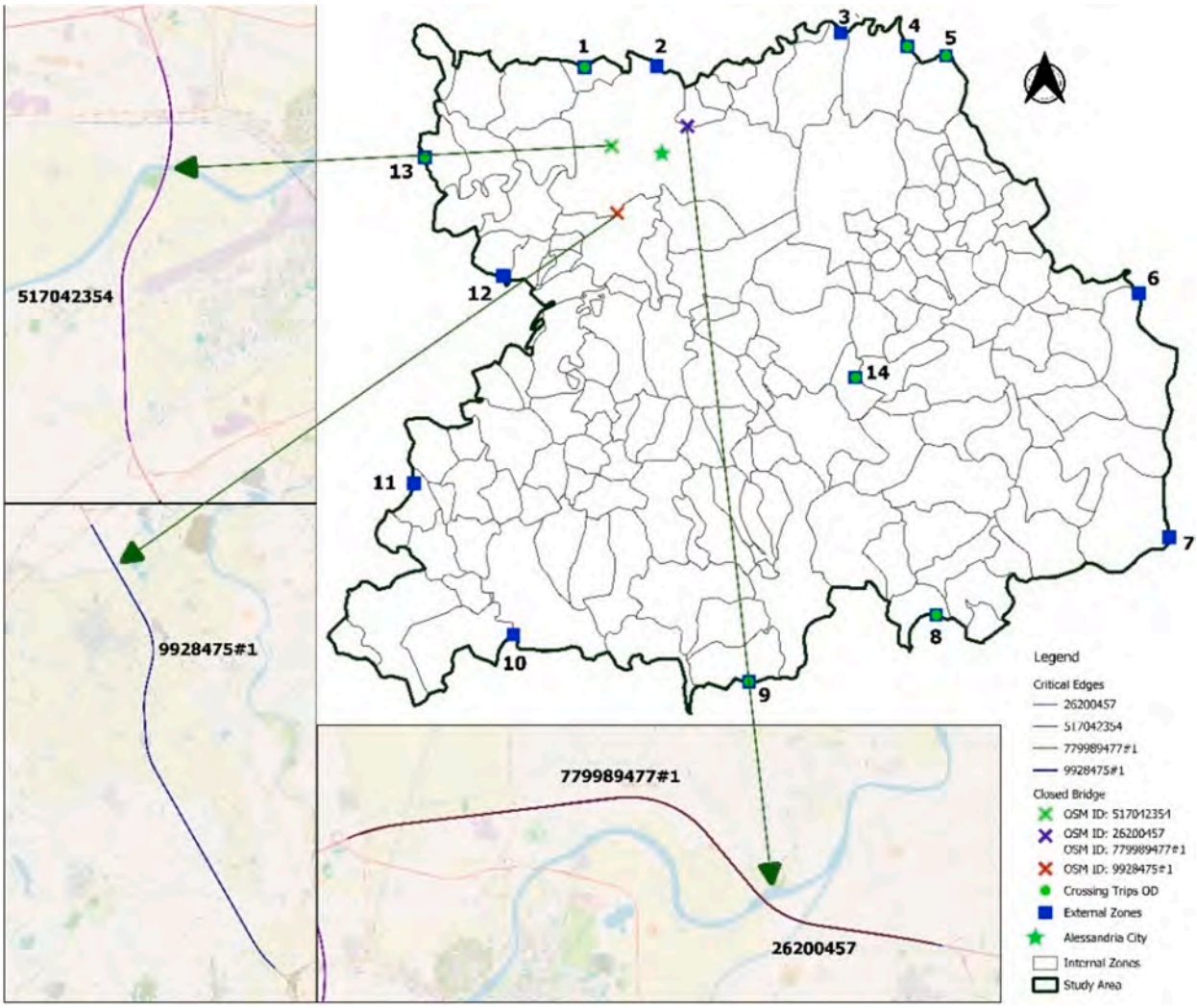

Fig. 11. Critical bridge edges (based on Max of Difference Weighted Time with Demand).

physical-bridge ranking derived from the original edge-based analysis is presented in Table 3.

As shown in Table 3, the two indicators provide complementary perspectives on bridge criticality. Bridge 7, a local road bridge over the Orba River, ranks first according to PDWT, with a maximum increase of 266.78 %, but ranks seventh when the affected travel demand is considered. Conversely, Bridge 4, located on the A21 motorway over the Tanaro River, ranks third according to PDWT but first according to the demand-weighted indicator, with a maximum value of 1,026,110 s. Bridges 1, 6, and 8, all located on motorway links, also rank highly when travel demand is incorporated. These results are consistent with the edge-level findings presented in Fig. 8–Fig. 11 and emphasize the distinction between severe relative impacts on individual O–D pairs and large absolute impacts affecting heavily travelled O–D relationships.

To examine whether the edge-based ranking remains representative when each physical bridge is treated as a complete infrastructure unit, 12 additional disruption scenarios were generated. In each scenario, all road-network edges associated with one physical bridge were closed simultaneously, while the same baseline O–D demand and incremental assignment settings were maintained. The resulting route-level and network-level indicators for these complete physical-bridge closure scenarios are reported in Table 4.

The results in Table 4 show a high degree of consistency with the bridge ranking derived from the edge-based analysis. Based on the demand-weighted indicator, Bridge 4 remains the most critical bridge, followed by Bridges 1 and 6, while Bridge 8 remains fourth. These four motorway bridges occupy the same leading positions in both the edge-based aggregation and complete physical-bridge closure analyses. Only limited changes occur among bridges with lower demand-weighted impacts; for example, Bridges 7 and 9 change from seventh and sixth positions in Table 3 to sixth and seventh positions in Table 4, respectively. This indicates that grouping and simultaneously closing all network edges belonging to a physical bridge does not materially alter the identification of the most critical bridges.

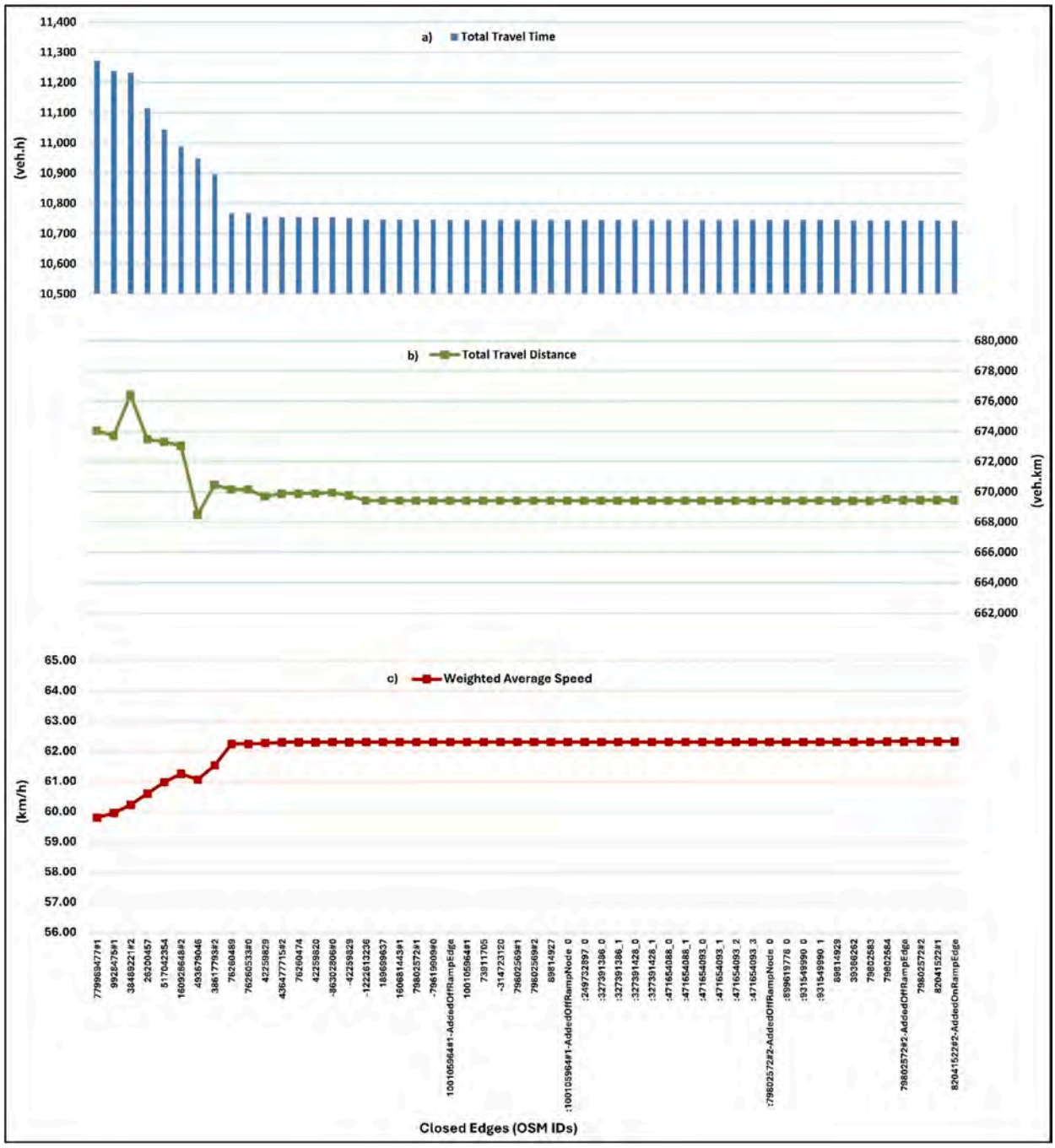

Fig. 12. Network performance indicators under bridge-edge closure scenarios: (a) total travel time (veh.h), (b) total travel distance (veh.km), and (c) weighted average speed (km/h), ordered by total travel time.

Although the route-level ranking remains largely stable, the complete closure of some physical bridges produces stronger network-wide effects than the closure of a single constituent edge. As reported in Table 4, Bridge 6 produces the highest total travel time among the physical-bridge scenarios, reaching 11,734 veh.h, together with the highest total travel distance of 680,517.7 veh.km and the lowest weighted average speed of 57.99 km/h. Bridge 4 similarly results in a total travel time of 11,653 veh.h and a total travel distance of 678,028.1 veh.km. These results indicate that closing all network edges representing a physical bridge can intensify network-wide traffic impacts even when the route-level criticality ranking remains broadly unchanged.

Overall, the physical-bridge analysis supports the robustness of the original edge-based screening for identifying the most critical structures while providing a more appropriate unit for practical prioritization. The edge-based analysis remains useful for isolating the

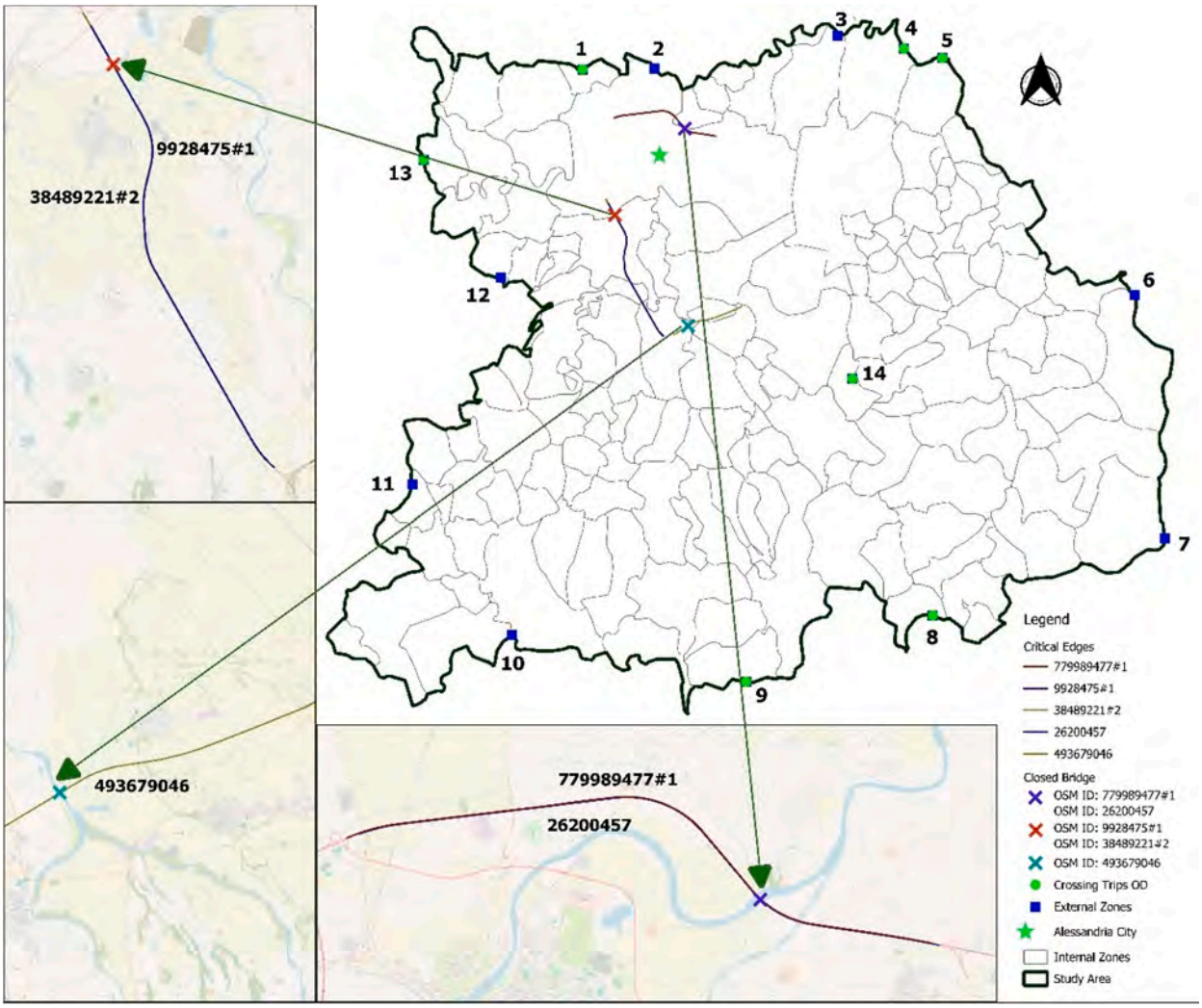

Fig. 13. Critical bridge edges (based on Total Travel Time).

Table 3
Physical-bridge ranking derived from edge-based route-level indicators.

Bridge ID	Road Class	River	Max of Percentage Difference Weighted Time (%)	PDWT Rank	Max of Difference Weighted Time * Number of Trips (sec)	Demand-Weighted Rank
1	motorway	Tanaro	128.05	2	896,496	2
2	secondary	Tanaro	43.18	7	2822	8
3	trunk	Tanaro	4.81	11	256	11
4	motorway	Tanaro	91.97	3	1,026,110	1
5	primary	Bormida	46.93	6	30,064	5
6	motorway	Bormida	66.79	5	826,356	3
7	local	Orba	266.78	1	6677	7
8	motorway	Orba	84.39	4	297,870	4
9	primary	Orba	34.95	8	6848	6
10	trunk	Tanaro	4.97	10	356	10
11	trunk	Tanaro	2.26	12	256	12
12	local	Tanaro	12.54	9	524	9

marginal effects of individual network links and maintaining computational scalability, whereas the physical-bridge closure analysis represents the complete loss of the infrastructure asset. The principal criticality patterns are preserved between the two analyses, particularly for the highly trafficked motorway bridges.

Table 4
Results and ranking of the physical-bridge closure scenarios based on route. and network-level indicators.

Bridge ID	Max of Percentage Difference Weighted Time (%)	PDWT Rank	Max of Difference Weighted Time * Number of Trips (sec)	Demand-Weighted Rank	Total Travel Time (veh.h)	Total Travel Distance (veh.km)	Weighted Average Speed (km/h)
1	127.59	2	892,428	2	11,288	676419.6	59.92
2	43.18	7	2822	8	10,746	669425.7	62.29
3	4.81	11	223	12	10,743	669436.3	62.32
4	91.98	3	1,024,536	1	11,653	678028.1	58.18
5	46.95	6	30,241	5	10,789	670425.8	62.14
6	67.00	5	828,763	3	11,734	680517.7	57.99
7	264.94	1	9244	6	10,765	670113.6	62.25
8	84.52	4	302,156	4	11,108	669432.3	60.27
9	34.95	8	6855	7	10,763	670418.3	62.29
10	4.97	10	378	10	10,742	669425.0	62.32
11	2.26	12	256	11	10,745	669406.7	62.30
12	12.53	9	524	9	10,743	669486.2	62.32

5.4. Comparison with topological bridge ranking

To assess the added value of considering traffic demand and flow redistribution in bridge criticality assessment, the physical-bridge ranking was compared with a purely topological evaluation of the road network. Global network efficiency was selected as the benchmark indicator, as it measures network performance based on the shortest-path distances between all pairs of nodes and can also be applied when disruptions result in disconnected node pairs (Latora and Marchiori, 2001). The indicator has also been applied in road-network robustness assessment to quantify changes in network accessibility under network perturbations (Kozhabek and Chai, 2025).

For the baseline network and each of the 12 physical-bridge closure scenarios, global efficiency was calculated as:

$$E_{glob} = \frac{1}{N(N-1)} \sum_{i \neq j} \frac{1}{d_{ij}} \tag{11}$$

where N is the total number of network nodes, and d_{ij} is the shortest-path distance between network nodes i and j, considering all pairs of network nodes. For disconnected node pairs, $1/d_{ij}$ is set to zero. This formulation therefore allows the effect of both increased shortest-path distances and loss of connectivity to be represented within the same indicator (Latora and Marchiori, 2001).

For each scenario, all network edges associated with the corresponding physical bridge were excluded, and global efficiency was recalculated. The topological impact of each bridge closure was then expressed as the percentage loss in global efficiency relative to the baseline network:

$$\Delta E_{glob}(\%) = \frac{E_{glob,baseline} - E_{glob,closure}}{E_{glob,baseline}} * 100 \tag{12}$$

The bridges were ranked in descending order of efficiency loss and compared with the demand-weighted ranking obtained from the incremental macroscopic traffic assignment (Table 4). Table 5 presents the efficiency loss and corresponding rankings for the 12 physical bridges.

The topological assessment produced a different criticality pattern from the demand-weighted analysis. Bridge 5 produced the

Table 5
Comparison of physical-bridge rankings based on topological efficiency and demand-weighted traffic assignment.

Bridge ID	Efficiency Loss (%)	Topological Rank	Demand-Weighted Rank	Rank Difference
1	0.045	11	2	9
2	0.076	6	8	−2
3	0.046	10	12	−2
4	0.075	7	1	6
5	1.312	1	5	−4
6	0.114	4	3	1
7	0.251	2	6	−4
8	0.073	8	4	4
9	0.181	3	7	−4
10	0.070	9	10	−1
11	0.025	12	11	1
12	0.113	5	9	−4

largest global efficiency loss (1.312 %) and was therefore ranked first topologically, followed by Bridges 7 and 9. In contrast, the demand-weighted analysis ranked Bridges 4, 1, 6, and 8 as the four most critical bridges. Particularly notable differences were observed for Bridge 1, which moved from 11th in the topological ranking to 2nd in the demand-weighted ranking, and Bridge 4, which moved from 7th to 1st. Conversely, Bridge 5 moved from 1st in the topological assessment to 5th when travel demand was considered.

The relatively small global efficiency losses for most bridge closures are consistent with the large size and redundancy of the analyzed road network. The closure of an individual bridge changes the shortest paths of only a subset of all network node pairs, while alternative connections remain available for most of the network. Nevertheless, these relatively small structural changes do not necessarily correspond to limited traffic impacts, since the topological assessment treats node pairs independently of the amount of travel demand between them.

The correspondence between the two rankings was further evaluated using Spearman's rank correlation coefficient. A weak positive association was obtained ($\rho = 0.273$, $p = 0.391$), indicating limited correspondence between the two bridge rankings. Fig. 14 further illustrates the differences between the topological efficiency ranking and the demand-weighted traffic assignment ranking.

Overall, the comparison shows that a purely topological assessment does not reproduce the same bridge prioritization obtained from the demand-weighted analysis. While global efficiency identifies bridges that are structurally important for maintaining short network connections, the macroscopic traffic assignment additionally accounts for the spatial distribution of travel demand and the redistribution of traffic following a closure. The differences between the two rankings therefore highlight the relevance of incorporating traffic demand and route redistribution when identifying critical bridges for transport-network operation.

5.5. Traffic-demand sensitivity analysis

To evaluate the sensitivity of the physical-bridge ranking to variations in the adopted traffic demand, particularly whether the identified criticality of motorway bridges is strongly dependent on the assumed motorway crossing demand, the motorway crossing trips, introduced in section 3.2, were varied by −50 %, −25 %, −10 %, +10 %, +25 %, and + 50 % relative to the baseline demand, while the internal and external demand components were kept unchanged. This range provides a robustness test of the bridge prioritization under substantial variations in the motorway demand estimates used in the analysis. For each demand level, the baseline network and the 12 physical-bridge closure scenarios were reassigned using the same incremental assignment procedure. Each bridge was then ranked based on the maximum Difference Weighted Time with Demand, consistently with the physical-bridge ranking presented in Section 5.3.

Table 6 shows that the ranking remained largely stable across the tested demand range. Bridges 1, 4, 6, and 8 occupied the first four positions under all demand scenarios, although the order of Bridges 1, 4, and 6 varied. Bridge 8 remained fourth in every scenario, while Bridge 5 remained fifth. Greater variations were observed among the lower-ranked bridges. The stability of the overall ranking across the tested demand variations is further illustrated in Fig. 15.

The correspondence between each modified-demand ranking and the baseline ranking was further evaluated using Spearman's rank correlation coefficient. Strong positive correlations were obtained for all scenarios, ranging from $\rho = 0.839$ to 0.979, with all correlations statistically significant ($p < 0.001$). The lowest correspondence occurred for the + 25 % scenario ($\rho = 0.839$), while the + 10 % scenario showed the highest correlation ($\rho = 0.979$).

Although the ranking remained relatively stable, the magnitude of the demand-weighted impacts varied with the crossing-demand level. As shown in Fig. 16 for the four consistently highest-ranked bridges, the maximum Difference Weighted Time with Demand generally increased as motorway crossing demand increased. Thus, the assumed crossing-demand level affects the magnitude of the estimated disruption impacts, as expected, but the consistently high ranking of the most critical motorway bridges is not solely driven by the baseline crossing-demand assumption. Their persistence among the highest-ranked bridges even when motorway crossing demand is reduced by up to 50 % supports the robustness of their identification as critical elements of the network.

6. Conclusion

Road networks are vital for supporting daily mobility, facilitating the movement of goods, and serving as critical lifelines during emergencies by ensuring regional connectivity. However, road networks, particularly bridges, are increasingly vulnerable to natural, technological and manmade disasters. Damage or failure of such infrastructure can severely disrupt connectivity, hinder emergency response operations, and delay post-disaster recovery efforts, ultimately undermining both societal resilience and overall mobility.

This study introduced a scalable and computationally efficient network modeling methodology for prioritizing bridge monitoring and retrofitting under disruption scenarios by integrating publicly available datasets, hazard information, and simplified macroscopic traffic simulation. Using the Alessandria case study, a flood-prone region in northern Italy, the methodology demonstrated how the functional significance of bridges, measured through their impact on regional mobility, can complement traditional structural assessments. The results show that certain bridge failures, particularly on motorway segments, can cause disproportionate disruptions to mobility, justifying their prioritization in resilience planning.

The analysis was conducted using open-source tools, including SUMO and QGIS. Traffic demand was assigned to baseline and disrupted road network scenarios using an incremental macroscopic traffic assignment approach, which can approximate user equilibrium conditions by assuming randomness in route choice. From assigned routes and network traffic flows, two classes of performance indicators were derived to assess the impact of each simulated bridge closure. The analysis revealed that specific bridges along major motorways are especially critical from a network performance perspective. The physical-bridge closure analysis confirmed that the principal criticality patterns identified from individual bridge-edge closures were preserved when complete bridges were closed.

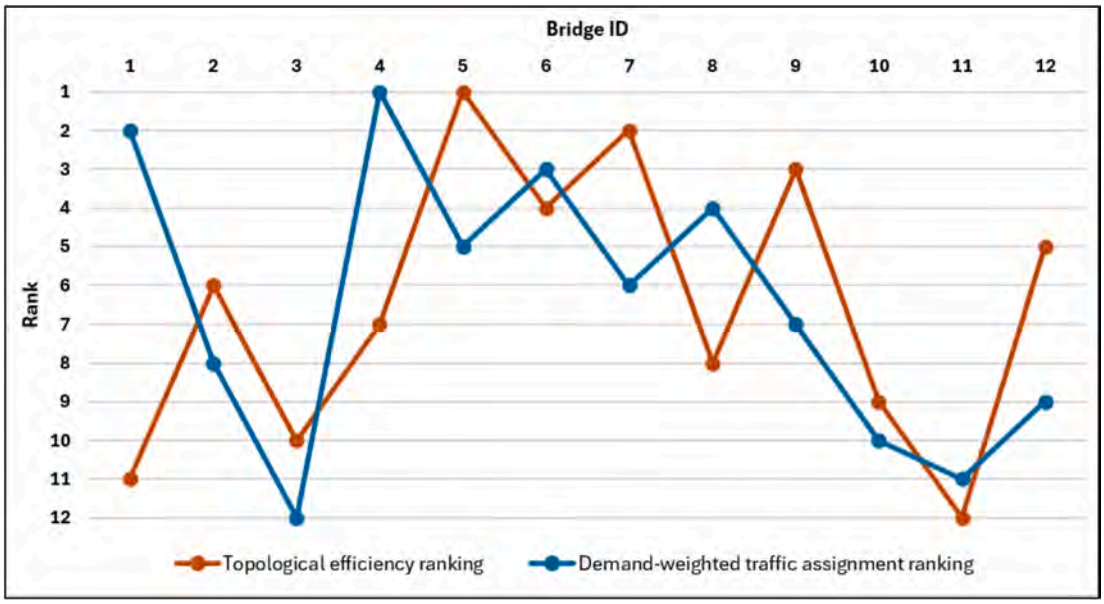

Fig. 14. Comparison of physical-bridge rankings obtained from topological efficiency and demand-weighted traffic assignment.

Table 6
Physical-bridge ranking under different motorway crossing-demand scenarios.

Bridge ID	−50 %	−25 %	−10 %	Baseline	+10 %	+25 %	+50 %
1	3	3	2	2	2	3	2
2	10	9	9	8	9	12	8
3	11	10	10	12	10	8	10
4	2	1	1	1	1	2	1
5	5	5	5	5	5	5	5
6	1	2	3	3	3	1	3
7	7	7	7	6	7	7	7
8	4	4	4	4	4	4	4
9	6	6	6	7	6	6	6
10	9	10	11	10	10	9	9
11	12	10	12	11	10	10	12
12	8	8	8	9	8	11	11

Comparison with a topological assessment showed limited correspondence between the rankings, highlighting the relevance of considering traffic demand and route redistribution, while the traffic-demand sensitivity analysis showed that the most critical motorway bridges remained highly ranked across substantial variations in motorway crossing demand. By iteratively simulating bridge-edge and physical-bridge closures in the mathematical model and evaluating the resulting traffic disruptions, the study developed a ranking system for identifying high-priority bridges for monitoring and retrofitting.

This approach is reproducible and transferable to other regions and may support decision-making, especially under budgetary constraints. It contributes to infrastructure resilience planning by identifying high-impact bridges using quantifiable mobility metrics, enabling authorities to target investments more effectively.

Several enhancements could improve the detail level and applicability of this framework. Incorporating dynamic flood propagation models and real-time data (e.g., rainfall, sensor-based traffic monitoring) would allow for time-dependent disruption scenarios. In addition, future work should consider spatially correlated failures involving the simultaneous disruption of multiple bridges and road segments within the same floodplain and extend the methodology to restoration-based analyses by jointly considering the edges representing each physical bridge. This would enable the evaluation of priority interventions in large-scale flood scenarios, although such approaches would require a large number of possible disruption combinations to be considered, making the analysis more complex (Li et al., 2024). Integrating economic loss estimation would enable cost-benefit analysis of retrofitting interventions. Future work could also extend the methodology to mesoscopic or agent-based traffic simulations, which would better capture individual travel behaviour and adaptive routing strategies in detailed studies at the local level. Additionally, expanding the traffic demand to include other trip purposes beyond commuter Home-Based Work (HBW) and Home-Based Education (HBE) trips, and covering non-peak periods or seasonal conditions, would increase the comprehensiveness of the analysis. The proposed methodology is not limited to a specific temporal demand scenario and can be applied using alternative data sources, including floating car data (FCD), traffic counts, mobile phone data, or calibrated O–D matrices, to represent different periods of the day or year. Higher-resolution demand

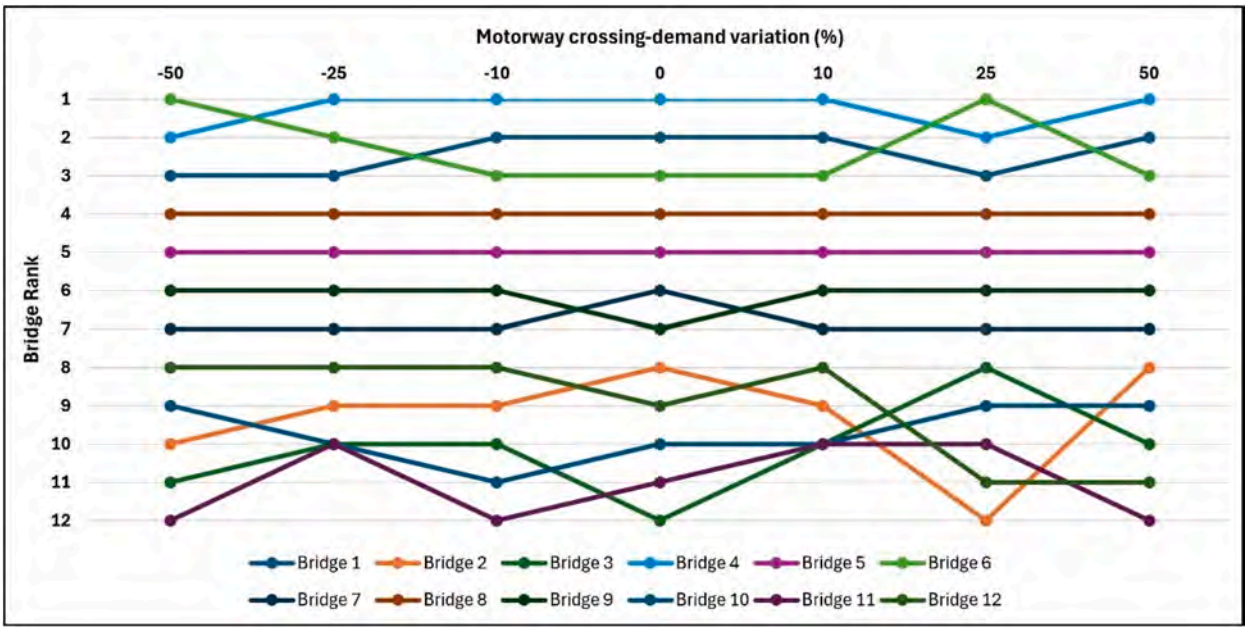

Fig. 15. Variation in physical-bridge ranking under different motorway crossing-demand scenarios.

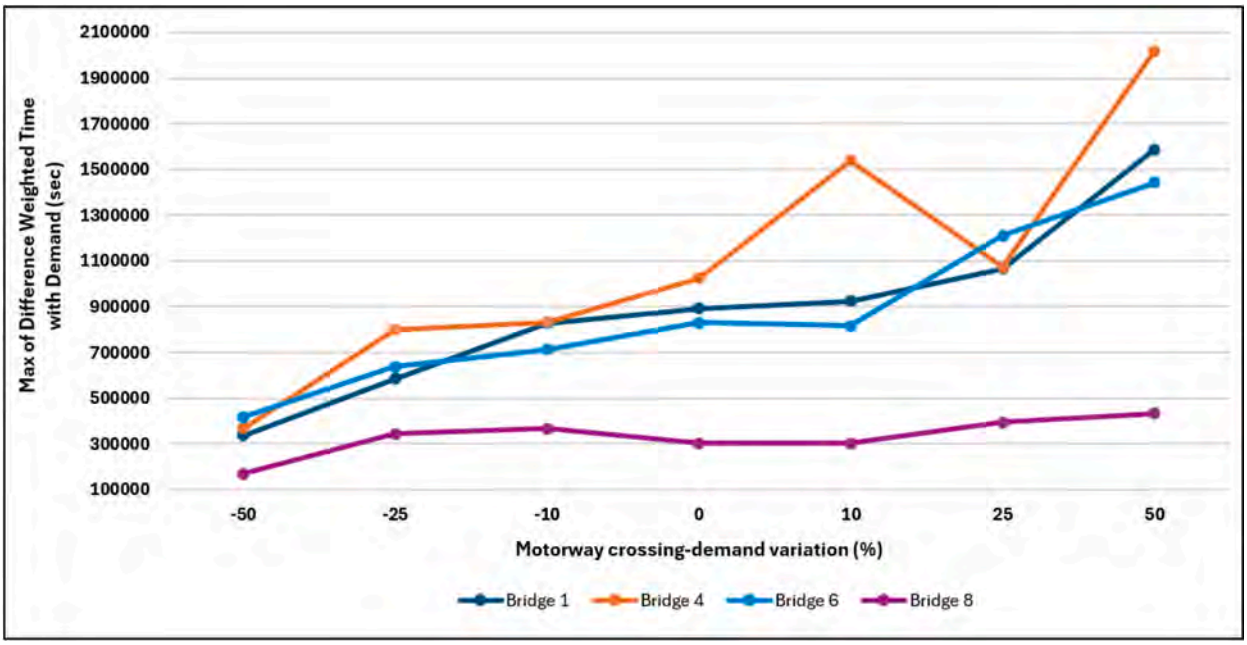

Fig. 16. Maximum Difference Weighted Time with Demand for the consistently highest-ranked bridges under different motorway crossing-demand scenarios.

inputs and finer zoning systems may further improve the robustness of the resulting bridge prioritization. In such cases, the resulting prioritization of critical bridges may vary depending on the temporal and spatial distribution of the adopted demand. Finally, the framework could be adapted to multi-hazard contexts, such as landslides or earthquakes, and applied to larger regional networks.

CRediT authorship contribution statement

Amirehsan Charlang Bakhtyari: Writing – review & editing, Writing – original draft, Visualization, Validation, Software, Methodology, Formal analysis, Data curation, Conceptualization. **Francesco Deflorio:** Writing – review & editing, Writing – original

draft, Visualization, Validation, Supervision, Project administration, Methodology, Conceptualization.

Declaration of competing interest

The authors declare the following financial interests/personal relationships which may be considered as potential competing interests: [Francesco Deflorio reports partial financial support was provided by Ministry of University and Research (PRIN 2022 program). If there are other authors, they declare that they have no known competing financial interests or personal relationships that could have appeared to influence the work reported in this paper].

Acknowledgements

This study was partially carried out within the FLOOD@ROAD project funded by the Ministero dell'Università e della Ricerca –within the PRIN 2022 program (D.D.104 02/02/2022). This manuscript reflects only the authors' views and opinions, and the Ministry cannot be considered responsible for them.

Appendix

Table A. 1 lists the entry and exit points to the study area along with their related road edge and class.

Table A
1- Entry and Exit points.

ID	Name	Road Class	Latitude	Longitude
1	A26_Autostrada dei Trafori	motorway	44.9778437	8.54564034
2	SS494_Strada Alessandria	primary	44.9789083	8.62686787
3	SS211_Strada statale della Lomellina	primary	45.0058918	8.83484837
4	A7_Autostrada dei Giovi-Serravalle	motorway	44.9953213	8.91024785
5	A21_Autostrada dei Vini	motorway	44.9877889	8.95392025
6	SP111	secondary	44.7969352	9.17150843
7	SP147	secondary	44.6016105	9.20474144
8	A7_Autostrada dei Giovi-Serravalle	motorway	44.5395146	8.94337585
9	A26_Autostrada dei Trafori	motorway	44.4858357	8.73351167
10	SP334_Strada provinciale del Sassello	primary	44.5224518	8.46925598
11	SP30	secondary	44.64271	8.3564144
12	SP240	secondary	44.8099838	8.45497758
13	A21_Autostrada dei Vini	motorway	44.9043332	8.365863
14	A7_Autostrada dei Giovi-Serravalle	motorway	44.7295531	8.85211617

2 lists the 12 physical bridges considered in the bridge-level analysis, including their assigned bridge ID, road name, river, and geographical location.

Table A
2- Bridge locations.

Bridge ID	Road/Bridge Name	Road Class	River	Latitude	Longitude
1	A26-Autostrada dei Trafori	motorway	Tanaro	44.9144898	8.57660896
2	SP10-Ponte Karlovac	secondary	Tanaro	44.9148613	8.60170752
3	SS10racc	trunk	Tanaro	44.93485369	8.61930017
4	A21-Strada dei Vini	motorway	Tanaro	44.930728	8.661877
5	Via Marengo	primary	Bormida	44.90561147	8.64519507
6	A26-Autostrada dei Trafori	motorway	Bormida	44.860747	8.5832393
7	SP181	local	Orba	44.83290261	8.63152307
8	A26/A7	motorway	Orba	44.77168291	8.66654389
9	SP179	primary	Orba	44.75737557	8.66174915
10	SS10racc	trunk	Tanaro	44.93524207	8.61367437
11	SS10racc	trunk	Tanaro	44.93054685	8.63698488
12	Strada Carlo Forlanini	local	Tanaro	44.93644159	8.62402902

Table A.3 presents a subset of O–D pairs for which the Percentage Difference Weighted Time (as defined by Eq. (6) in Section 2.5) exceeds 50 % in disrupted scenarios.

Table A
3- Percentage Difference Weighted Time.

Bridge ID	Closed Bridge Edge (OSM IDs)	From TAZ	To TAZ	Number of Trips	Disrupted Weighted Time (sec)	Baseline Weighted Time (sec)	Difference Weighted Time (sec)	Percentage Difference Weighted Time (%)
7	−42259829	006,047	006021#1	1	695.78	189.70	506.08	266.78
7	42,259,829	006,075	006,047	6	615.11	184.22	430.89	233.90
7	−42259829	006,047	006,075	1	591.28	207.12	384.16	185.48
7	42,259,829	006,075	006,054	1	944.21	358.65	585.56	163.27
1	517,042,354	EX_01	006,140	1	1955.80	857.62	1098.18	128.05
1	517,042,354	EX_01	006,047	1	1131.05	524.52	606.53	115.64
4	779989477#1	006,003	006,068	3	476.00	247.96	228.04	91.97
4	779989477#1	006,141	EX_13	1	758.26	411.05	347.21	84.47
8	38617793#2	006,030	006,114	1	558.34	302.81	255.53	84.39
4	26,200,457	006,129	006,174	2	1784.85	1003.27	781.58	77.90
8	38617793#2	006,174	006,140	4	1099.94	620.27	479.67	77.33
4	26,200,457	EX_01	006,174	49	2039.56	1165.53	874.03	74.99
8	38617793#2	006,183	006,114	2	128.89	73.97	54.92	74.25
4	779989477#1	006,174	EX_01	37	1901.00	1125.83	775.17	68.85
8	493,679,046	006,140	006,174	9	1142.38	683.17	459.21	67.22
6	38489221#2	006021#1	006,121	4	1340.59	803.74	536.85	66.79
4	779989477#1	006,174	006,068	4	2584.36	1554.26	1030.11	66.28
6	38489221#2	006,003	006,049	11	1620.31	977.39	642.92	65.78
6	38489221#2	006,003	006,029	13	1130.36	690.12	440.24	63.79
6	38489221#2	006,003	006,014	3	2227.63	1361.28	866.35	63.64
4	779989477#1	006,163	EX_13	2	613.01	379.25	233.76	61.64
4	779989477#1	EX_05	006,068	1	3147.95	1953.10	1194.85	61.18
4	779989477#1	006,174	006,163	2	2026.94	1260.55	766.38	60.80
8	38617793#2	006,186	006,121	1	2452.80	1539.88	912.92	59.29
8	38617793#2	006,114	006,127	1	4.33	2.72	1.61	59.19
8	38617793#2	006,127	006,114	1	4.33	2.72	1.61	59.19
4	779989477#1	006,174	006,141	1	2177.06	1374.75	802.31	58.36
4	779989477#1	006,174	006,076	1	2685.51	1708.32	977.19	57.20
6	38489221#2	006,003	006,121	68	1955.83	1260.42	695.41	55.17
6	38489221#2	006,029	006,121	1	390.53	251.68	138.85	55.17
4	779989477#1	EX_03	006,068	1	2756.88	1781.93	974.95	54.71
6	38489221#2	EX_01	006,012	2	1978.86	1282.84	696.03	54.26
6	38489221#2	006,051	006,121	1	2855.66	1853.08	1002.57	54.10
6	38489221#2	006,012	006,121	2	865.28	562.22	303.06	53.90
6	38489221#2	006,003	006,162	7	1735.88	1134.02	601.87	53.07
4	26,200,457	EX_01	006053#0	3	2187.52	1430.18	757.34	52.95
6	38489221#2	006,003	006,169	1	1943.47	1270.77	672.70	52.94
1	517,042,354	EX_01	006021#1	1	1294.73	847.17	447.56	52.83
4	779989477#1	006,075	006,076	1	1758.51	1151.69	606.82	52.69
4	779989477#1	006,174	006,122	1	1907.28	1254.29	652.99	52.06
6	38489221#2	010,051	EX_09	1	715.87	470.88	244.99	52.03
4	779989477#1	EX_05	006,076	1	3161.50	2084.58	1076.93	51.66
1	160928648#2	006,121	EX_01	5	2489.64	1643.60	846.04	51.47
6	38489221#2	006,003	010,008	6	3001.59	1982.96	1018.63	51.37
6	38489221#2	006,003	010,051	2	2668.08	1766.75	901.33	51.02
1	160928648#2	006,141	EX_01	1	742.50	492.17	250.33	50.86
4	26,200,457	006,129	006053#0	1	1902.44	1267.91	634.53	50.05

Table A. 4 presents a subset of O–D pairs for which the Difference Weighted Time with Demand (as defined by Eq. (7) in Section 2.5) is notably high. These values reflect the compounded weighted travel time increases multiplied by the number of trips between each O–D pair.

Table A
4- Difference Weighted Time with Demand.

Bridge ID	Closed Bridge Edge (OSM IDs)	From TAZ	To TAZ	Number of Trips	Disrupted Weighted Time (sec)	Baseline Weighted Time (sec)	Difference Weighted Time (sec)	Difference Weighted Time * Number of Trips (sec)
4	26,200,457	EX_13	EX_05	1111	2956	2032	924	1,026,110
4	779989477#1	EX_05	EX_13	1111	2930	2052	878	975,389

(continued on next page)

Table A (*continued*)

Bridge ID	Closed Bridge Edge (OSM IDs)	From TAZ	To TAZ	Number of Trips	Disrupted Weighted Time (sec)	Baseline Weighted Time (sec)	Difference Weighted Time (sec)	Difference Weighted Time * Number of Trips (sec)
1	517,042,354	EX_01	EX_09	750	3851	2655	1195	896,496
6	9928475#1	EX_09	EX_01	750	3683	2582	1102	826,356
1	160928648#2	EX_09	EX_01	750	3394	2582	813	609,741
6	38489221#2	EX_01	EX_09	750	3353	2655	697	522,811
8	38617793#2	EX_04	EX_09	544	4069	3521	548	297,870
8	493,679,046	EX_09	EX_04	544	4054	3535	519	282,579
6	38489221#2	006,003	EX_09	172	3378	2350	1028	176,750
8	493,679,046	EX_08	EX_04	1329	3793	3706	87	115,685
6	9928475#1	EX_08	EX_04	1329	3770	3706	65	85,803
6	38489221#2	006,003	006,121	68	1956	1260	695	47,288
4	26,200,457	EX_13	006,174	50	2626	1768	858	42,924
4	26,200,457	EX_01	006,174	49	2040	1166	874	42,828
6	9928475#1	EX_09	006,003	97	2700	2268	432	41,922
8	38617793#2	006,174	EX_09	44	3383	2499	884	38,898
8	493,679,046	EX_14	EX_04	830	2055	2013	42	34,811
6	9928475#1	EX_14	EX_04	830	2052	2013	39	32,590
5	76,260,489	EX_05	EX_13	1111	2079	2052	27	30,064
5	76260533#0	EX_05	EX_13	1111	2079	2052	27	30,064
8	493,679,046	EX_09	006,174	29	3461	2425	1036	30,049
4	779989477#1	006,174	EX_01	37	1901	1126	775	28,681
6	9928475#1	006,001	006,003	171	1337	1182	155	26,562
4	779989477#1	006,174	EX_13	42	2397	1774	624	26,191
6	9928475#1	006,121	006,003	117	1526	1329	197	23,026
8	38617793#2	EX_04	EX_08	1329	3716	3700	16	21,417
8	493,679,046	006,121	006,174	50	1879	1455	424	21,178
6	38489221#2	006,003	006,114	259	624	546	78	20,129
8	38617793#2	EX_04	EX_14	830	1850	1827	23	19,156
4	26,200,457	EX_02	006,174	34	1734	1187	547	18,594
5	436477715#2	EX_13	EX_05	1111	2049	2032	16	18,176
5	76,260,474	EX_13	EX_05	1111	2049	2032	16	18,176
1	517,042,354	EX_13	EX_05	1111	2049	2032	16	18,143
6	9928475#1	EX_08	006,003	164	3171	3082	89	14,617
4	779989477#1	EX_06	006,003	82	2207	2029	178	14,572
8	38617793#2	EX_06	006,003	82	2201	2029	172	14,123
4	26,200,457	EX_06	006,003	82	2201	2029	172	14,092
6	38489221#2	EX_06	006,003	82	2197	2029	168	13,808
5	436477715#2	EX_06	006,003	82	2195	2029	166	13,622
5	76,260,474	EX_06	006,003	82	2195	2029	166	13,622
1	517,042,354	EX_01	006,001	20	2233	1562	670	13,407
5	76,260,489	EX_06	006,003	82	2191	2029	162	13,268
5	76260533#0	EX_06	006,003	82	2191	2029	162	13,268
6	38489221#2	006,003	006,001	143	1139	1046	93	13,249
6	38489221#2	EX_13	EX_05	1111	2043	2032	11	12,510
8	38617793#2	006,174	006,121	26	1897	1425	472	12,274
1	160928648#2	EX_05	EX_13	1111	2062	2052	10	11,266
8	493,679,046	EX_13	EX_05	1111	2042	2032	10	10,854
5	76,260,489	006,174	EX_02	30	1503	1154	349	10,485
5	76260533#0	006,174	EX_02	30	1503	1154	349	10,485

Data availability

Research Link Provided

Dataset and Traffic Flow Simulation in Wide Road Network to Evaluate Bridges in Flooding Events Registered in the Alessandria Region (Reference data) (Mendeley Data)

References

Aghababaei, M.T. (Siavash), Costello, S.B., Ranjitkar, P., 2021. Measures to evaluate post-disaster trip resilience on road networks. Journal of Transport Geography 95, 103154. 10.1016/j.jtrangeo.2021.103154.

Akbari, V., Sayarshad, H.R., 2022. Integrated and coordinated relief logistics and road recovery planning problem. Transp. Res. Part D: Transp. Environ. 111, 103433. https://doi.org/10.1016/j.trd.2022.103433.

Associazione Italiana Società Concessionarie Autostrade e Trafori, Traffic flow on motorways [WWW Document], n.d. URL https://www.aiscat.it/2023/12/29/aiscat-informazioni-edizione-semestrale-1-2-2023/ (accessed 2.28.25).

Balijepalli, C., Oppong, O., 2014. Measuring vulnerability of road network considering the extent of serviceability of critical road links in urban areas. J. Transp. Geogr. 39, 145–155. https://doi.org/10.1016/j.jtrangeo.2014.06.025.

Berdica, K., 2002. An introduction to road vulnerability: what has been done, is done and should be done. Transp. Policy 9, 117–127. https://doi.org/10.1016/S0967-070X(02)00011-2.

Bhattacharjee, G., Baker, J.W., 2023. Using global variance-based sensitivity analysis to prioritise bridge retrofits in a regional road network subject to seismic hazard. Struct. Infrastruct. Eng. https://doi.org/10.1080/15732479.2021.1931892.

Boeing, G., Ha, J., 2024. Resilient by design: Simulating street network disruptions across every urban area in the world. Transp. Res. A Policy Pract. 182, 104016. https://doi.org/10.1016/j.tra.2024.104016.

Bruneau, M., Chang, S.E., Eguchi, R.T., Lee, G.C., O'Rourke, T.D., Reinhorn, A.M., Shinozuka, M., Tierney, K., Wallace, W.A., Von Winterfeldt, D., 2003. A framework to quantitatively assess and enhance the seismic resilience of communities. Earthq. Spectra 19, 733–752. https://doi.org/10.1193/1.1623497.

Buzzi, A., Tartaglione, N., Malguzzi, P., 1998. Numerical simulations of the 1994 piedmont flood: role of orography and moist processes. Mon. Weather Rev. 126, 2369–2383. https://doi.org/10.1175/1520-0493(1998)126%3C2369:NSOTPF%3E2.0.CO;2.

Cascetta, E., 2009. Transportation Systems Analysis: Models and Applications, Springer Optimization and Its Applications. Springer US, Boston, MA. 10.1007/978-0-387-75857-2.

Charlang Bakhtyari, A., Carboni, A., Deflorio, F., Ferraro, M., Sica, L., 2025. Impact assessment on spatial connectivity and simulation of traffic flows under flood-related road network disruptions. Sustain. Cities Soc. 135, 107003. https://doi.org/10.1016/j.scs.2025.107003.

de Dios Ortuzar, J., Willumsen, L.G., 2011. Modeling Transport, 4th Edition.

Deflorio, F., Carboni, A., Renzi, E., Palermo, G., Nucci, F.D., Zampino, S., 2024. Analysis of road networks resilience in simulated scenarios of seismic events. International Association for Earthquake Engineering, Milan.

Evans, B., Chen, A.S., Djordjevic, S., Webber, J., Gonz, A., 2020. Investigating the effects of pluvial flooding and climate change on traffic flows in barcelona and bristol. Sustainability. https://doi.org/10.3390/su12062330.

Galvez-Hernandez, P., Dai, Y., Muntaner, C., 2025. The DANA disaster: unraveling the political and economic determinants for Valencia's floods devastation. Int. J. Equity Health 24, 64. https://doi.org/10.1186/s12939-025-02435-0.

Ganin, A.A., Kitsak, M., Marchese, D., Keisler, J.M., Seager, T., Linkov, I., 2017. Resilience and efficiency in transportation networks. Sci. Adv. 3, e1701079. https://doi.org/10.1126/sciadv.1701079.

Gao, L., Liu, X., Liu, Y., Wang, P., Deng, M., Zhu, Q., Li, H., 2019. Measuring road network topology vulnerability by Ricci curvature. Physica A 527, 121071. https://doi.org/10.1016/j.physa.2019.121071.

Gauthier, P., Furno, A., Faouzi, N.E.E., 2018. Road Network Resilience: how to Identify critical Links Subject to Day-to-Day Disruptions. Transp. Res. Rec. https://doi.org/10.1177/0361198118792115.

Geoportal of Piedmont, Administrative areas [WWW Document], n.d. URL https://www.geoportale.piemonte.it/geonetwork/srv/ita/catalog.search#/metadata/r_piemon:56e122a6-f3b1-4436-a49c-2b96dab53239 (accessed 2.28.25).

Geoportal of Piedmont, Arpa Piemonte, Floodable areas [WWW Document], n.d. URL https://www.geoportale.piemonte.it/geonetwork/srv/ita/catalog.search#/metadata/arlpa_to:07.03.01_ai-D_2013-10-08:14:38 (accessed 3.3.25).

Geoportal of Piedmont, Arpa Piemonte, Hydrographic basins [WWW Document], n.d. URL https://www.geoportale.piemonte.it/geonetwork/srv/ita/catalog.search#/metadata/arlpa_to:12.01.01-D_2011-06-21-11:30 (accessed 2.28.25).

Istituto Nazionale di Statistica, Administrative areas [WWW Document], n.d. URL https://www.istat.it/notizia/confini-delle-unita-amministrative-a-fini-statistici-al-1-gennaio-2018-2/ (accessed 3.16.25).

Istituto Nazionale di Statistica, Commuting Matrices [WWW Document], n.d. URL https://www.istat.it/non-categorizzato/matrici-di-contiguita-distanza-e-pendolarismo/ (accessed 2.28.25).

Jafari, E., Gemar, M.D., Juri, N.R., Duthie, J., 2015. Investigation of centroid connector placement for advanced traffic assignment models with added network detail. Transp. Res. Rec: J. Transp. Res. Board 2498, 19–26. https://doi.org/10.3141/2498-03.

Kopiika, N., Di Bari, R., Argyroudis, S., Ninic, J., Mitoulis, S.-A., 2025. Sustainability and resilience-driven prioritisation for restoring critical infrastructure after major disasters and conflict. Transp. Res. Part D: Transp. Environ. 139, 104592. https://doi.org/10.1016/j.trd.2025.104592.

Kozhabek, A., Chai, W.K., 2025. Robustness assessment of urban road networks in densely populated cities. Appl. Netw. Sci. 10, 29. https://doi.org/10.1007/s41109-025-00707-w.

Lanari, R., Reale, D., Bonano, M., Verde, S., Muhammad, Y., Fornaro, G., Casu, F., Manunta, M., 2020. Comment on "Pre-Collapse Space Geodetic Observations of Critical Infrastructure: The Morandi Bridge, Genoa, Italy" by Milillo et al. (2019). Remote Sensing 12, 4011. 10.3390/rs12244011.

Latora, V., Marchiori, M., 2001. Efficient behavior of small-world networks. Phys. Rev. Lett. 87, 198701. https://doi.org/10.1103/PhysRevLett.87.198701.

Li, P., Wang, Z., Zhao, B., Becker, T., Soga, K., 2024. Surrogate modeling for identifying critical bridges in traffic networks under earthquake conditions. Transp. Res. Part D: Transp. Environ. 104512. https://doi.org/10.1016/j.trd.2024.104512.

Liu, L., Frangopol, D.M., Mondoro, A., Yang, D.Y., 2018. Sustainability-informed bridge ranking under scour based on transportation network performance and multiattribute utility. J. Bridg. Eng. 23, 04018082. https://doi.org/10.1061/(ASCE)BE.1943-5592.0001296.

Lopez, P.A., Wiessner, E., Behrisch, M., Bieker-Walz, L., Erdmann, J., Flotterod, Y.-P., Hilbrich, R., Lucken, L., Rummel, J., Wagner, P., 2018. Microscopic Traffic simulation using SUMO. In: 2018 21st International Conference on Intelligent Transportation Systems (ITSC). Presented at the 2018 21st International Conference on Intelligent Transportation Systems (ITSC), pp. 2575–2582. https://doi.org/10.1109/ITSC.2018.8569938.

Mandarino, A., Luino, F., Turconi, L., Faccini, F., 2021. Urban geomorphology of a historical city straddling the Tanaro River (Alessandria, NW Italy). J. Maps 17, 29–41. https://doi.org/10.1080/17445647.2020.1746420.

Mashrur, N., Kameshwar, S., 2025. Ranking paths in road networks for equitable improvement in connectivity during disasters. Transp. Res. Part D: Transp. Environ. 140, 104611. https://doi.org/10.1016/j.trd.2025.104611.

Mattsson, L.-G., Jenelius, E., 2015. Vulnerability and resilience of transport systems – a discussion of recent research. Transp. Res. A Policy Pract. 81, 16–34. https://doi.org/10.1016/j.tra.2015.06.002.

Ouyang, M., Tian, H., Wang, Z., Hong, L., Mao, Z., 2019. Critical infrastructure vulnerability to spatially localized failures with applications to chinese railway system. Risk Anal. 39, 180–194. https://doi.org/10.1111/risa.12708.

Peng, Y., Xu, M., Li, G., Chen, A., 2024. Sequencing post-disruption concurrent restoration via a network flow approach. Transp. Res. Part D: Transp. Environ. 133, 104234. https://doi.org/10.1016/j.trd.2024.104234.

Pregnolato, M., Ford, A., Wilkinson, S.M., Dawson, R.J., 2017. The impact of flooding on road transport: a depth-disruption function. Transp. Res. Part D: Transp. Environ. 55, 67–81. https://doi.org/10.1016/j.trd.2017.06.020.

Pyatkova, K., Chen, A.S., Butler, D., Vojinović, Z., Djordjević, S., 2019. Assessing the knock-on effects of flooding on road transportation. J. Environ. Manage. 244, 48–60. https://doi.org/10.1016/j.jenvman.2019.05.013.

Rapelli, M., Casetti, C., Gagliardi, G., 2022. Vehicular traffic simulation in the city of turin from raw data. IEEE Trans. Mob. Comput. 21, 4656–4666. https://doi.org/10.1109/TMC.2021.3075985.

Rapelli, M., Casetti, C., Gagliardi, G., 2019. TuST: from Raw Data to Vehicular Traffic Simulation in Turin, in: 2019 IEEE/ACM 23rd International Symposium on Distributed Simulation and Real Time Applications (DS-RT). Presented at the 2019 IEEE/ACM 23rd International Symposium on Distributed Simulation and Real Time Applications (DS-RT), IEEE, Cosenza, Italy, pp. 1–8. 10.1109/DS-RT47707.2019.8958652.

Shahdani, F.J., Santamaria-Ariza, M., Sousa, H.S., Coelho, M., Matos, J.C., 2022. Assessing flood indirect impacts on road transport networks applying mesoscopic traffic modelling: the case study of santarém Portugal. Appl. Sci. 12, 3076. https://doi.org/10.3390/app12063076.

Silva-Lopez, R., Baker, J.W., 2022. Use of corridors to select bridges to retrofit in road networks in seismic regions. Sustain. Resilient Infrastruct. https://doi.org/10.1080/23789689.2022.2108594.

SUMO, Dynamic User Assignment [WWW Document], 2025. URL https://sumo.dlr.de/docs/Demand/Dynamic_User_Assignment.html#introduction (accessed 12.9.25).
SUMO, Marouter [WWW Document], 2025. URL https://sumo.dlr.de/docs/marouter.html (accessed 12.9.25).
Taylor, M., 2017. Vulnerability Analysis for Transportation Networks - 1st Edition. Elsevier..
Tran, H., Robert, D., Gunarathna, P., Setunge, S., 2024. Estimating cost of bridge closure for bridge network rehabilitation priorities. J. Constr. Eng. Manag. 150, 04024071. https://doi.org/10.1061/JCEMD4.COENG-14619.
Tsapakis, I., Cheng, T., Bolbol, A., 2013. Impact of weather conditions on macroscopic urban travel times. J. Transp. Geogr. 28, 204–211. https://doi.org/10.1016/j.jtrangeo.2012.11.003.
Westrum, R., 2006. A typology of resilience situations. Resilience Engineering: Concepts and Precepts 55–65.
Wikipedia, 2024 Spanish floods [WWW Document], 2024. URL https://en.wikipedia.org/wiki/2024_Spanish_floods#Casualties_and_damage (accessed 4.16.25).
Wu, Y., Hou, G., Chen, S., 2021. Post-earthquake resilience assessment and long-term restoration prioritization of transportation network. Reliability Eng. Syst. Safety 211, 107612. https://doi.org/10.1016/j.ress.2021.107612.
Zamanifar, M., Hartmann, T., 2021. Decision attributes for disaster recovery planning of transportation networks; a case study. Transp. Res. Part d: Transp. Environ. 93, 102771. https://doi.org/10.1016/j.trd.2021.102771.
Zhao, L., Wang, S., Wei, J., Chen, R., 2022. Impacts of land use on urban road network vulnerability. J. Urban Plan. Develop. 148, 04022032. https://doi.org/10.1061/(ASCE)UP.1943-5444.0000862.
Zhu, Y., Ozbay, K., Yang, H., Zuo, F., Sha, D., 2021. Modeling and simulation of cascading failures in transportation systems during hurricane evacuations. J. Adv. Transp. 2021, 1–12. https://doi.org/10.1155/2021/5599073.